THESIS FOR THE DEGREE OF DOCTOR OF PHILOSOPHY

Impact of Surface Loading on Stress and Seismicity Modulation in Global Subduction Zones

YITING CAI

Department of Physics and Astronomy
Onsala Space Observatory
CHALMERS UNIVERSITY OF TECHNOLOGY

Gothenburg, Sweden 2026

Impact of Surface Loading on Stress and Seismicity Modulation in Global Subduction Zones

YITING CAI
ISBN 978-91-8103-413-4

Doktorsavhandlingar vid Chalmers tekniska högskola
Ny serie nr. 5870
ISSN 0346-718X
Department of Physics and Astronomy
Onsala Space Observatory
Chalmers University of Technology
SE-412 96 Gothenburg
Sweden
Telephone: +46 (0)31-772 1000

Cover:
Schematic overview of surface-loading-driven stress perturbations in a subduction zone setting.

This thesis has been prepared using LaTeX. In the preparation of this thesis, ChatGPT was used to improve readability, review chapter structure, and support brainstorming on societal impact. The author drafted and revised the thesis. AI-assisted suggestions were critically reviewed and edited by the author to ensure accuracy and appropriateness. The author takes full responsibility for the final content.

Chalmers Reproservice
Gothenburg, Sweden 2026

Impact of Surface Loading on Stress and Seismicity Modulation in Global Subduction Zones

YITING CAI
Department of Physics and Astronomy
Chalmers University of Technology

Abstract

Surface mass redistribution from hydrological, atmospheric, and oceanic processes continually deforms the solid Earth and produces stress perturbations that are small in amplitude but coherent in space and periodic in time. This thesis examines whether such loading-induced stress variations are mechanically relevant for earthquake occurrence in subduction zones, and evaluates them in a tectonic context.

The regional study of the Kuril Islands-Japan region resolves loading-induced stress changes onto the megathrust geometry to compute monthly Coulomb failure stress changes from hydrological, atmospheric, and non-tidal ocean loading. A weak but statistically significant correlation is found between multi-loading-induced Coulomb stress variations and seismicity in some areas, with the clearest signal in the shallow southern Kuril segment near Hokkaido. The global study uses satellite gravimetry data from the GRACE and GRACE-FO missions to compute monthly loading-induced stress variations in the upper 50 km, and projects them onto principal tectonic stress directions inferred from earthquake focal mechanisms. The projected stress perturbations are then compared with background seismicity. Results reveal faulting- and region-dependent patterns of stress modulation and seismic response across global subduction zones.

Together, the results indicate that modest, periodic stress variations from surface loading can measurably modulate earthquake occurrence in parts of the subduction system, and that both fault-geometry-based and ambient-stress-based perspectives are useful for interpreting this modulation.

Keywords: Surface loading, tectonic stress, seismicity, subduction zone

To Wenchuan, where this journey began

Acknowledgements

Geophysics has always amused me with its language, full of words like stress, fault, failure, and perturbation. They sound negative, yet they describe the processes that shape our planet. In some ways, my PhD journey followed a similar theme: it was challenging, nonlinear, and full of change. Between a global pandemic and a change of supervision, it was not a smooth path, but looking back, I am proud of how these experiences shaped me and made the journey unique and memorable.

I would first like to express my deepest gratitude to Maxime Mouyen for his guidance, support, and mentorship during the early years of my PhD. His scientific curiosity, kindness, and integrity have left a lasting impression on me, both as a researcher and as a person. The change of supervision was unexpected, but it also pushed me to become more independent, adaptable, and proactive. Even afterward, he continued to support and encourage me, and I deeply value the friendship and trust we have maintained. I wish him all the best in the new chapter of his life.

My sincere thanks go to Karine Le Bail, who began as my co-supervisor and later took on the role of main supervisor. Her thoughtful guidance, steady encouragement, and kindness made a real difference in the later stages of my PhD. The monthly PhD lunches she initiated created a warm and supportive space for sharing ideas, struggles, and tasty French pastries.

I am deeply grateful to Roland Bürgmann, who welcomed me into his research group after a cold email and became both a supervisor and collaborator. Working with him has been an incredibly enriching experience. His breadth of knowledge scientific rigor, generosity with ideas, and encouragement guided me through many uncertain moments, and I feel very fortunate to have had his mentorship.

I would also like to thank Rüdiger for his role as both my examiner and line manager, and for giving me the opportunity to work on this project. I am also deeply grateful to everyone who supported and encouraged me along the way, whether by opening new doors, discussing research with me, or inviting me to share my work. Their kindness and generosity made me feel welcomed and part of a wider community during this transition.

I would like to thank my colleagues and fellow PhD students at Chalmers for their support, good company, and humor that brightened so many long days in the office. I will always remember the warmth and sense of community that made those years feel more joyful. My stays at Berkeley were also made especially lovely and inspiring by the wonderful people I met there. I am very thankful for their kindness, friendship, and the many memorable moments that made that time incredibly special to me.

I also want to thank my friends, both near and far, who brought balance, joy, and comfort to these years. Through shared meals, deep talks, laughter, encouragement, and simply being there, they reminded me that life is bigger than work and made this journey feel lighter and richer.

Finally, my deepest gratitude goes to my family, Yijun, Yanping, and Yonggao, for their love and belief in me. And to Andreas, who has seen every high and low of this journey and, through it all, stood beside me with care, humor, and understanding.

Yiting Cai
Gothenburg, April 2026

Publications

This thesis is based on the work contained in the following papers:

I Yiting Cai and Maxime Mouyen (2024). Loading-induced stress variation on active faults and seismicity modulation in the Kuril Islands-Japan region. *Earth and Planetary Science Letters*, **643**, 118904. DOI: https://doi.org/10.1016/j.epsl.2024.118904

II Yiting Cai, Roland Bürgmann, Eva Boergens, Maxime Mouyen, Kristel Chanard, and Karine Le Bail (2026). Global modulation of stress and seismicity in subduction interfaces by surface loads. *Journal of Geophysical Research: Solid Earth*. Submitted

III Alexandru Mihai Lapadat, Hubert Pierzchała, Osmari Aponte, Yiting Cai, Iwona Kudłacik, Eduard Ilie Nastase, Maciej Lackowski, and Jan Kapłon (2026). Automatic S-wave arrival timing in GNSS instantaneous velocity data. *Journal of Geodesy*. under revision

Contents

Part I
Overview

Chapter 1

Introduction

Throughout most of human history, earthquakes were interpreted through mythological frameworks rather than scientific ones. In Greek mythology, Poseidon, the god of the sea and the Earth Shaker, was believed to unleash earthquakes as expressions of divine anger (Burkert, 1985). Similarly, in ancient China, earthquakes were commonly interpreted as warnings or punishments from heaven, arising from disruptions in the yin-yang balance (Cai, 2015). Such narratives framed earthquakes as unpredictable, uncontrollable, and profoundly destructive forces of nature. Although modern science has transformed our contemporary understanding of the Earth, this longstanding perception remains partially valid: earthquakes continue to rank among the most devastating natural hazards, and many aspects of their behavior remain difficult to predict (Ismail-Zadeh, 2013; Jordan et al., 2011; Mulargia et al., 2017; UNDRR, 2026).

The emergence of modern seismology has replaced mythological explanations with a physical framework rooted in plate tectonics. It is now well established that most earthquakes result from unstable slip on faults after tectonic stresses have accumulated in the lithosphere, particularly along plate boundaries, causing a sudden release of stored energy (Scholz, 2019; Turcotte and Schubert, 2002). Foundational theories such as the elastic rebound theory, combined with advances in our understanding of fault friction and rupture dynamics, provide a robust conceptual basis for interpreting seismic events (Dieterich, 1979; Kanamori and Brodsky, 2004). Over the past several decades, improvements in seismic instrumentation, dense global and regional seismic networks, space-based geodesy, and numerical modeling have dramatically enhanced our ability to detect earthquakes, constrain fault geometry, and characterize seismic sources (Shearer, 2019).

Despite these advances, critical gaps in knowledge remain. In particular, the timing of earthquakes, the mechanisms governing why some faults rupture while others creep or remain locked, and the role of small, often transient, stress perturbations in modulating fault stability are still not fully understood (Chen and Bürgmann, 2017; Gomberg et al., 1998; Harris, 2017; McLaskey, 2019). These unresolved questions fundamentally limit our ability to anticipate earthquake occurrence beyond long-term, probabilistic seismic hazard assessments (Jordan et al., 2011).

The societal consequences of these scientific uncertainties are substantial. Destructive earthquakes frequently result in extensive damage to infrastructure and significant loss of life. According to the World Health Organization (WHO, 2026), between 1998 and 2017 earthquakes and their associated cascading hazards, including tsunamis, landslides, and soil liquefaction, caused nearly 750,000 fatalities worldwide, accounting for more than half of all deaths from natural disasters during that period. During the same interval, more than 125 million people were affected globally (WHO, 2026). Beyond direct ground shaking, earthquakes can trigger a wide range of secondary hazards, such as landslides, avalanches, infrastructure failure, and tsunamis, which substantially amplify their overall societal impact.

Consequently, improving our understanding of earthquake processes is not only a scientific challenge but also a societal imperative. Enhanced knowledge of fault mechanics and earthquake triggering mechanisms contributes directly to improved disaster preparedness, more resilient building codes, and better-informed land-use planning (Day, 2012). Moreover, advances in earthquake science support sustainable economic development by reducing long-term losses due to damage and disruption and by strengthening the resilience of communities exposed to seismic risk (Coburn and Spence, 2003). One tangible outcome of advances in earthquake science is the development of earthquake early warning systems. These systems detect the initial, low-amplitude seismic waves generated near the earthquake source and rapidly estimate source parameters to issue alerts before the arrival of the more damaging ground shaking (Allen et al., 2009; Cremen and Galasso, 2020). Although early warning systems cannot predict earthquakes, they can provide seconds to tens of seconds of warning, allowing automated systems and individuals to take protective actions, such as stopping trains, shutting down critical infrastructure, or seeking cover (Allen and Melgar, 2019). Such systems highlight how improved physical understanding of earthquake processes can translate directly into societal benefits.

Beyond their societal relevance, earthquakes also provide a unique window into the Earth's interior. Direct observation of the Earth becomes increasingly infeasible with depth, making seismic waves the primary tool for probing internal structure (Shearer, 2019). By analyzing the propagation, reflection, and conversion of seismic waves, researchers have constrained the structure and composition of the crust, mapped discontinuities such as the Moho, and inferred temperature, composition, and deformation mechanisms within the mantle (Cammarano et al., 2003; Karato and Karki, 2001; Prodehl et al., 2013; Romanowicz, 2003; Stern, 2002). Earthquakes have also revealed complex processes such as metamorphic reactions, fluid migration, and stress redistribution within the crust and upper mantle (Ferrand et al., 2017; Freed, 2005; Halpaap et al., 2019; Hardebeck and

Okada, 2018; Jamtveit et al., 2018). Thus, seismicity is not only a hazard but also a fundamental observational tool for understanding Earth's dynamic interior.

Most earthquakes occur at tectonic plate boundaries, where long-term plate motions lead to the accumulation of stress on faults (Turcotte and Schubert, 2002). However, tectonic loading is not the only source of stress acting on faults. Non-tectonic processes such as surface mass redistribution continuously generate stress perturbations within the lithosphere (see Fig. 1.1). Over the past decades, numerous studies have examined whether such stress variations modulate seismicity in different tectonic settings. Representative examples include studies in California (Gao et al., 2000; Johnson et al., 2017), Alaska (Johnson et al., 2020), the New Madrid Seismic Zone (Craig et al., 2017), Japan (Heki, 2003), Taiwan (Hsu et al., 2021), the Himalayas (Bettinelli et al., 2008), and Nepal (Bollinger et al., 2007). Many of these studies report that non-tectonic stress perturbations of only a few kilopascals (kPa) can correlate with changes in seismicity rates, suggesting that faults in these regions are critically stressed and sensitive to small stress changes.

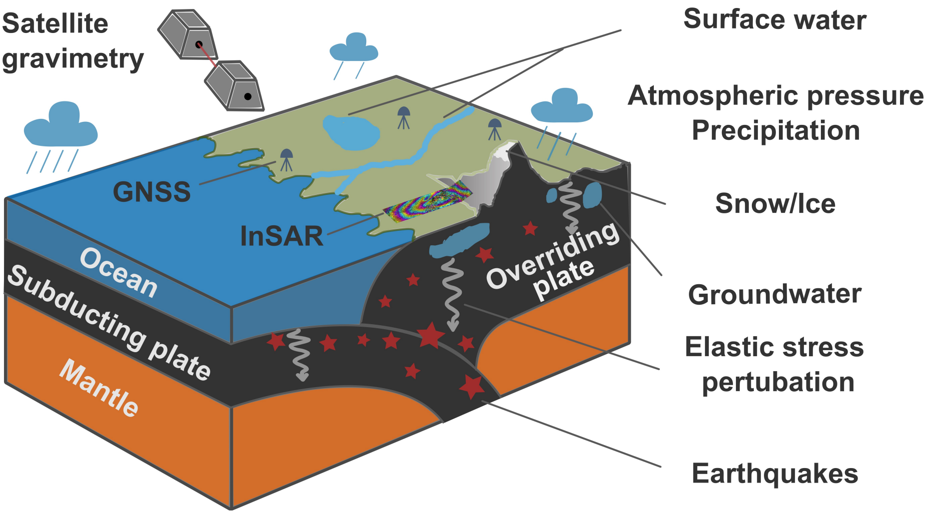

Fig. 1.1: *Schematic overview of surface-loading-driven stress perturbations in a subduction zone setting. Time-varying hydrological, atmospheric, and non-tidal ocean mass redistribute surface loads and generate (visco-)elastic stress changes that propagate into the lithosphere, perturbing the subsurface stress state and potentially modulating earthquake occurrence. Surface mass changes can be observed directly by satellite gravimetry (GRACE/GRACE-FO) and indirectly through deformation measured by GNSS and InSAR. In this thesis, GRACE/GRACE-FO products provide the primary constraint on surface mass redistribution used to compute loading-induced stress variations.*

At the same time, the existence and robustness of such correlations remain debated. Several studies have reported weak or absent correlations between periodic stress perturbations and earthquake occurrence, particularly for solid Earth tides (Beeler and Lockner, 2003; Vidale et al., 1998). Laboratory experiments investigating periodic loading and acoustic emissions similarly demonstrate that the response of fault slip to cyclic stress depends strongly on fault properties, loading rate, and the proximity of the system to failure (Bartlow et al., 2012; Colledge et al., 2023; Pignalberi et al., 2024). These results indicate that stress modulation is not universal, but conditional, reflecting the complex, nonlinear nature of fault systems. Consequently, identifying the physical mechanisms and conditions under which small stress perturbations influence seismicity remains an open problem.

This thesis addresses these challenges by investigating how surface loading–induced stress variations affect fault systems in subduction zones. By combining satellite-derived surface loading and physically grounded stress modeling with observations of seismicity, this work aims to improve our understanding of when and where loading-induced stress perturbations are relevant for earthquake occurrence, and how such effects can be robustly quantified.

1.1 Outline of the thesis

This thesis investigates whether stress perturbations associated with surface mass redistribution can contribute to measurable modulation of earthquake occurrence in subduction settings. The overview part is mainly presented as an introduction and discussion of two papers that evaluate loading-induced stress variations using two complementary perspectives (see Fig. 1.2): one resolves stress variations on the megathrust plane, and the other evaluates the stress changes by projecting them onto principal stress directions of the ambient tectonic stress. Then the stress perturbations are compared with the seismicity in the study regions. In addition, a third paper provides methodological context on earthquake observations by developing an automated framework for detecting S-wave arrivals and quantifying shaking parameters from high-rate GNSS velocity time series, illustrating how geodetic data can complement seismic measurements for rapid ground-motion characterization and monitoring applications. The chapters of the thesis provide the geological and physical background, introduce the relevant loading and seismicity data sets, describe the stress-evaluation procedures used in the papers, and discuss methodological choices that affect inference.

Chapter 2 introduces the tectonic setting relevant for the thesis, with emphasis on subduction zones and the structural and mechanical context in which earthquakes occur. It summarizes lithospheric structure, subduction-zone geometry, and the stress and fault concepts, including a description of background stress fields along global subduction margins. Chapter 3 introduces surface loading as a source of non-tectonic stress variation. It reviews the main loading processes,

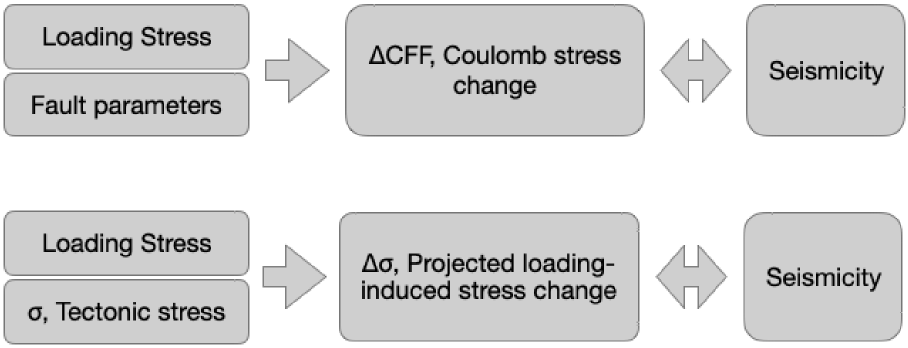

Fig. 1.2: *Conceptual overview of the two stress-evaluation frameworks used in this thesis. Top: fault-plane-based approach, where loading-induced stress tensors are resolved onto a defined fault plane to compute changes in shear and normal stress and the Coulomb failure stress change. Bottom: principal-axis-oriented approach, where the same stress tensors are projected onto the ambient principal stress directions inferred from focal mechanisms. In both cases, the resulting stress metrics are compared with background seismicity to assess potential modulation.*

outlines observational and model-based constraints on surface mass redistribution, and describes how loading-induced stress changes are characterized in space, time, and depth. Chapter 4 describes how loading-induced stress tensors are evaluated in a tectonic context. It introduces the two conceptual frameworks used in the appended papers: a fault-plane-based approach that resolves stresses onto subduction interfaces and computes Coulomb failure stress changes, and a principal-axis-oriented approach that projects stress perturbations onto principal stress directions inferred from earthquakes. Chapter 5 then describes how seismicity is treated as a response indicator. It discusses background seismicity and triggering concepts, earthquake catalog completeness and magnitude of completeness, and declustering strategies, highlighting how these methodological choices affect seismicity rate analyses and the interpretation of weak modulation signals. Chapter 6 provides short summaries of the appended papers. Chapter 7 synthesizes the implications of the thesis and the appended papers, discusses limitations and open questions, and outlines directions for future research.

Chapter 2

Tectonic framework and stress as a physical quantity

2.1 Plate tectonics

Plate tectonics[1] provides the framework for understanding the large-scale deformation of the Earth's outer shell. The lithosphere is divided into a number of rigid to semi-rigid plates (see Fig. 2.1) that move relative to one another over millions to hundreds of millions of years. These motions are driven primarily by mantle convection and gravitational forces acting on subducting slabs and elevated lithosphere. Plate interactions give rise to a wide range of geological processes, including earthquakes, volcanic activity, and mountain building, and thus form the fundamental context for stress accumulation and release in the Earth's crust.

The lithosphere constitutes the outermost mechanically coherent layer of the Earth and is composed of the crust together with the uppermost portion of the mantle. Its mechanically strong upper part can store elastic strain and fail brittlely, allowing stress to accumulate and be released during earthquakes. In contrast, the underlying asthenosphere deforms viscously and accommodates mantle flow.

Plate boundaries are commonly classified according to the relative motion between adjacent plates into convergent, divergent, and transform boundaries (see Fig. 2.2). Divergent boundaries occur where plates move apart and are typically associated with mid-ocean ridges, where new oceanic lithosphere is formed. Transform boundaries accommodate lateral plate motion through strike-slip faulting. Although they neither create new lithosphere nor recycle existing ones into the mantle, they are efficient sites of elastic strain accumulation and

[1] This chapter is broadly based on Turcotte and Schubert (2002), which serves as the general reference wherever other literature is not explicitly cited.

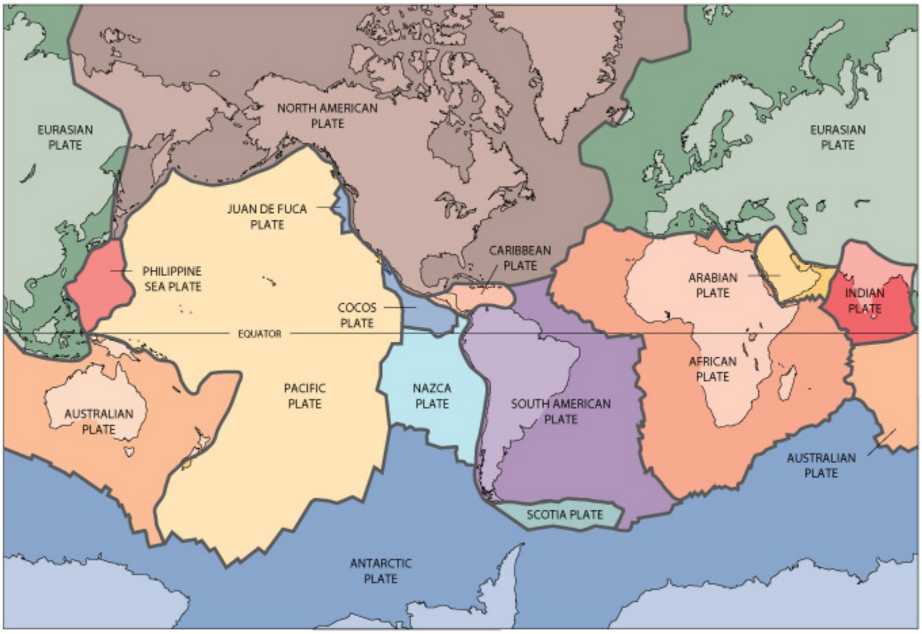

Fig. 2.1: *The main tectonic plates and their boundaries. Reproduced from* *https://pubs.usgs.gov/gip/dynamic/slabs.html.*

earthquake generation, for example along the San Andreas Fault system in California (Smith-Konter and Sandwell, 2009).

Convergent boundaries are characterized by plate convergence and are most commonly associated with subduction zones, where one plate is forced beneath another into the mantle. Subduction environments represent some of the most seismically active regions on Earth (Hayes et al., 2018). They play a central role in transmitting stress from deep lithospheric and mantle processes to the shallow crust and are therefore important for understanding earthquake generation and stress evolution in the lithosphere (Petricca and Carminati, 2016).

In some convergent settings, however, subduction is restricted when buoyant continental lithosphere enters the trench. This leads to continent–continent collision, in which convergence is accommodated by large-scale crustal shortening, thickening, and mountain building rather than slab descent. Although collision zones remain seismically active, deformation in these regions is typically more distributed and involves complex fault networks within the upper crust (Wang and Barbot, 2023; Zheng et al., 2017).

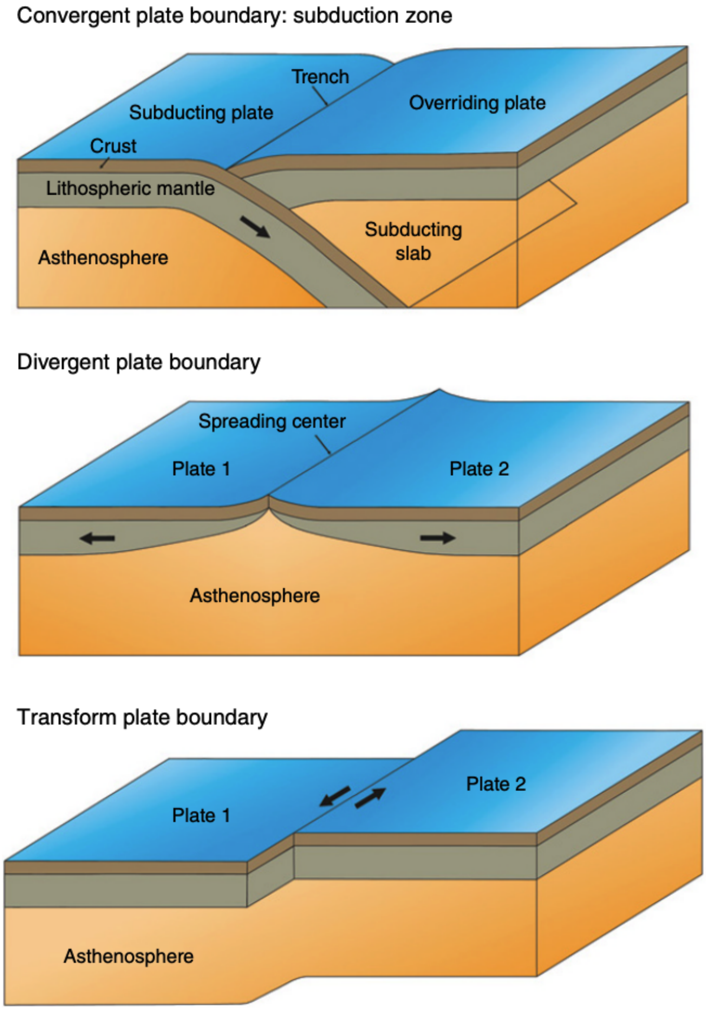

Fig. 2.2: *The three main types of plate boundaries: convergent, divergent, and transform boundaries. Reproduced from Duarte and Schellart (2016).*

2.2 Subduction zones

Subduction zones are a fundamental expression of convergent plate boundaries, where one tectonic plate is forced beneath another and descends into the mantle. In most cases, the subducting plate consists of relatively dense oceanic lithosphere, while the overriding plate may be either oceanic or continental. As convergence proceeds, deformation is accommodated across a complex system that includes the plate interface, the downgoing slab, the overriding plate, and the surrounding mantle. These systems play a central role in global tectonics and account for a large fraction of the Earth's seismic moment release (Stern, 2002).

As the subducting slab descends, it undergoes progressive metamorphic reactions that release water and other volatiles into the overlying mantle wedge. These fluids lower the solidus of mantle rocks, promoting partial melting and ultimately feeding arc volcanism. At the same time, the mechanical interaction between the converging plates leads to the accumulation of stress across a wide range of depths, from relatively shallow megathrust settings at roughly 5–50 km depth (Dixon and Moore, 2007; Kopp, 2013) to intermediate- and deep-focus seismicity within the descending slab down to nearly 700 km (Hayes et al., 2018; Scire et al., 2017). Subduction zones therefore host diverse styles of seismicity, from megathrust earthquakes at the plate interface to intermediate- and deep-focus earthquakes within the descending slab (Bilek and Lay, 2018).

Quantitative characterization of subduction zone geometry has been significantly advanced by the Slab2 model (Hayes et al., 2018, Fig. 2.3), which provides a global, three-dimensional representation of subducting slabs. Slab2 integrates multiple data sources, including active-source seismic profiles, receiver functions, earthquake hypocenter distributions, and seismic tomography, to map slab surfaces from near-trench depths to their deepest expressions in the upper mantle. Covering approximately 24 million square kilometers, the model offers a consistent framework for describing slab geometry across different tectonic settings (Hayes et al., 2018).

Accurate representations of slab geometry are essential for a wide range of applications, including earthquake and tsunami hazard assessment (Geist and Lynett, 2014; Pagani et al., 2014), as well as studies of mantle flow and lithosphere–asthenosphere interaction (Morishige and Honda, 2013). In the work related to this thesis, such models provide a critical geometric foundation for analyzing stress fields, fault systems, and the mechanical behavior of subduction zones across both shallow and deep environments.

2.3 Stress fields and fault systems

The Earth's lithosphere is subject to continuous stress loading arising from a combination of tectonic and non-tectonic processes. On a global scale, relative plate motions impose boundary forces that generate long-term stress accumu-

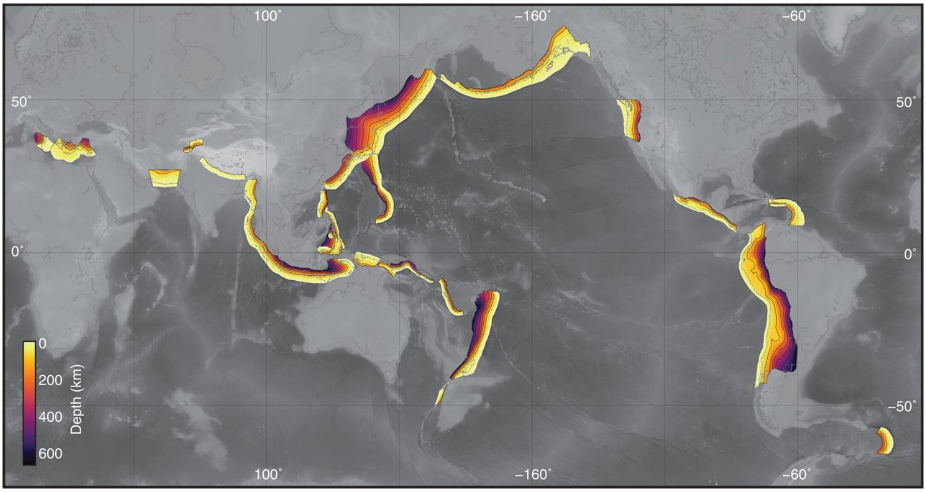

Fig. 2.3: *Global distribution of subduction zone geometries included in the Slab2 model, colored by depth. Reproduced from Hayes et al. (2018).*

lation within the crust and upper mantle. Superimposed on these plate-driven stresses are regional and local contributions from gravitational body forces, topography, density contrasts, mantle flow, and transient processes such as postseismic relaxation, surface loading, and fluid pressure variations (Zoback, 1992). Understanding how these stresses are distributed in space and evolve over time is important for interpreting crustal deformation, faulting, and earthquake occurrence.

Observations of the contemporary stress field demonstrate that stress orientation and faulting regime vary across tectonic environments. The global compilation provided by the World Stress Map (Heidbach et al., 2018, Fig. 2.4) reveals coherent large-scale patterns of maximum horizontal stress orientation that broadly reflect plate boundary forces, while also exhibiting substantial regional variability. This variability highlights the inherently heterogeneous nature of the lithospheric stress field (Heidbach et al., 2018; Zoback, 1992).

At any given point, the state of stress can be described by the stress tensor, which fully characterizes the magnitudes and orientations of stresses acting on all possible planes. For tectonic applications, it is often convenient to express the stress state in terms of the three principal stresses: the maximum (σ_1), intermediate (σ_2), and minimum (σ_3) principal stresses. As shown in Fig. 2.5, these quantities define the preferred orientations of faulting and provide a link between stress and observable fault kinematics (Heidbach et al., 2018). Both stress magnitude and orientation may vary with depth, reflecting changes in lithology, temperature, pressure, and dominant deformation mechanisms.

Faults represent localized zones of weakness within the crust where deforma-

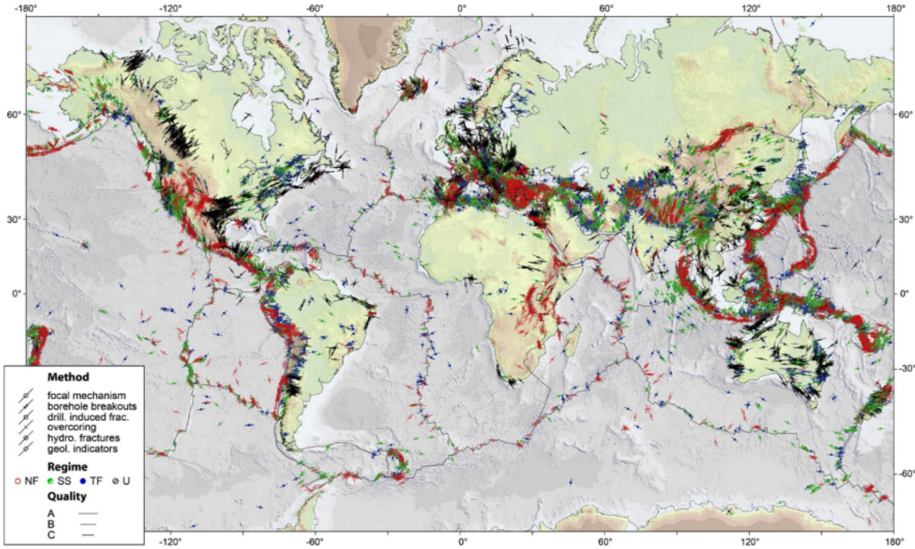

Fig. 2.4: *World Stress Map 2016, reproduced from Heidbach et al. (2018). Lines indicate the orientation of maximum horizontal stress. Colors represent faulting regimes: normal (red), strike-slip (green), thrust (blue), and unknown (black).*

tion is preferentially accommodated. The orientation of a fault relative to the ambient stress field strongly influences whether it is favorably oriented for slip and what style of faulting may occur. Fault is commonly described using strike, dip, and rake, which together specify the orientation of the fault plane and the direction of slip (Fig. 2.6).

While plate tectonics provides the kinematic framework for large-scale deformation, the localized stress fields would provide the information on which faults may be reactivated and earthquakes may occur. Stress is therefore not merely a conceptual construct but a measurable physical quantity that can be inferred from geological observations, seismic data, and geodetic measurements.

2.3.1 Stress field along global subduction-zone plate interfaces

In subduction zones, the interaction between plate-driven loading, slab geometry, rheological contrasts, and transient stress perturbations produces complex, depth-dependent stress fields (Hardebeck, 2015). While the World Stress Map provides a valuable global overview of present-day stress orientations, its coverage in subduction environments is spatially uneven and primarily reflects stress indicators within the uppermost 40 km of lithosphere (Heidbach et al., 2018), which is not enough to capture the state of stress in subduction zones.

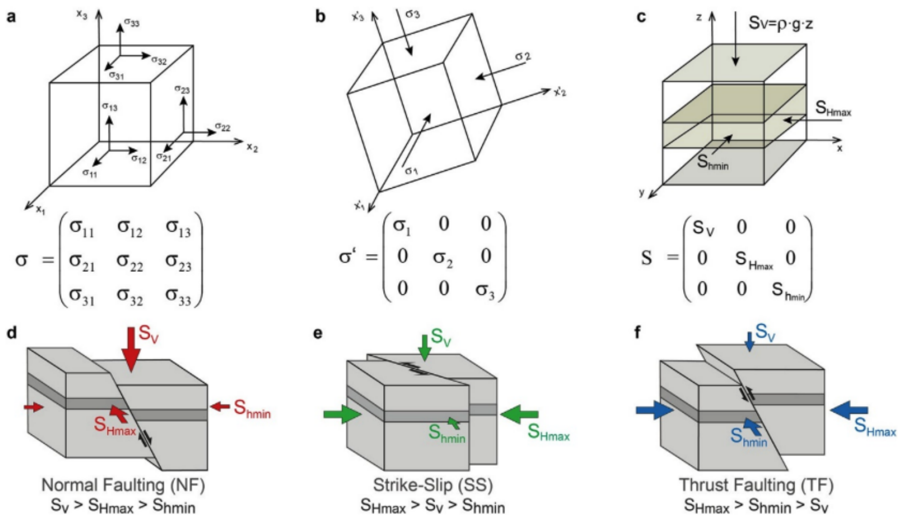

Fig. 2.5: *Stress tensor geometry, principal stresses, and idealized faulting regimes, reproduced from Heidbach et al. (2018). (a) Stress components acting on a unit cube, resolved into normal and shear stresses on each face. (b) Since the stress tensor is symmetric, a principal coordinate system exists in which shear stresses vanish and only the three principal stresses remain. (c) Assuming the vertical stress in the crust is a principal stress, the maximum and minimum horizontal stresses, S_{Hmax} and S_{hmin}, are the other principal stresses. In this reduced stress tensor, the stress state is described by the orientation of S_{Hmax} and the magnitudes of S_V, S_{Hmax}, and S_{hmin}. (d–f) Corresponding stress regimes: normal faulting ($S_V = \sigma_1$), strike-slip faulting ($S_V = \sigma_2$), and thrust faulting ($S_V = \sigma_3$).*

Previous studies show that stress in subduction zones varies strongly with tectonic domain and depth (Petricca and Carminati, 2016). The Hellenic subduction zone, for example, illustrates the strong spatial and depth-dependent variability of subduction-zone stress. Shallow seismicity includes both compressional and extensional faulting in different tectonic domains, whereas intermediate-depth (> 40 km) earthquakes within the Hellenic slab are commonly strike-slip to transpressional, with compression main axis broadly parallel to the arc and marked along-arc variability (Benetatos et al., 2004; Bohnhoff et al., 2005; Rontogianni et al., 2011; Shaw and Jackson, 2010). Another example is the northern Chile margin, where shallow seismicity on the coupled megathrust is dominated by reverse faulting and compression, whereas below the downdip end of interplate coupling the slab stress regime shifts and normal-faulting, downdip-extensive intraslab earthquakes become widespread (Bloch et al., 2018). More detailed

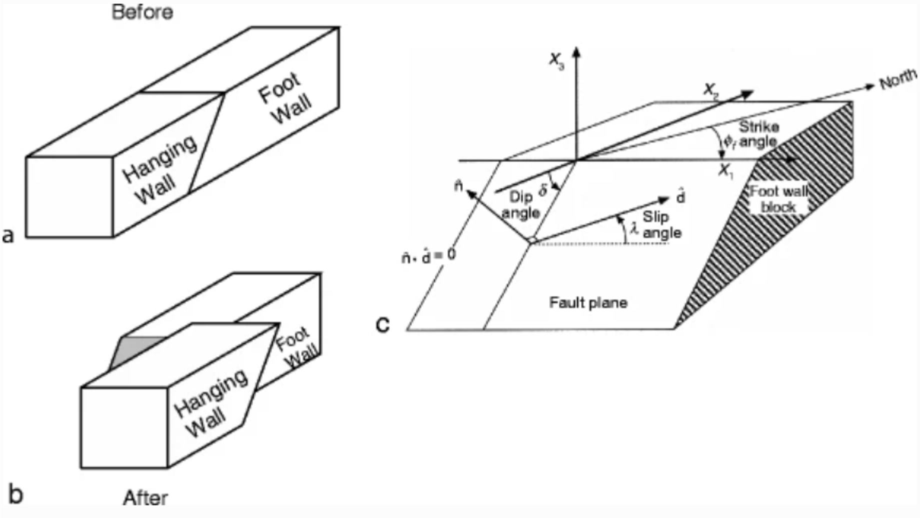

Fig. 2.6: *Schematic illustration of fault-block displacement and the definition of rupture geometry parameters, reproduced from Okal (2011). (a–b) Before and after sketches of the relative displacement of fault blocks across a fault during coseismic slip; the fault plane is shaded in panel (b). (c) Definition of strike (ϕ), dip (δ), and rake (λ), which describe the orientation of the fault plane and the direction of slip. The slip vector represents the motion of the hanging wall relative to the footwall.*

analyses further show that the Nazca slab exhibits depth-dependent stress partitioning within a double seismic zone: at shallow depths, the upper plane is downdip compressional and the lower plane downdip extensive, but at about 60–65 km depth the upper plane also becomes downdip extensive, while the lower plane remains extensive (Sippl et al., 2023). Intermediate-depth double seismic zones are not unique to Chile, but are also observed in other subduction zones such as Japan, the Aleutians, Tonga, and Central America (Florez and Prieto, 2019), where two parallel planes of earthquakes occur within the downgoing lithosphere. These double seismic zones show that stress can vary not only with depth along the slab, but also across its thickness; a commonly observed pattern is downdip-compressive earthquakes in the upper plane over downdip-extensive earthquakes in the lower plane, consistent with unbending-related stresses (Sippl et al., 2022). This further complicates the stress state within the intermediate-depth subducting slab. At greater depths, downdip compression becomes more common as the slab encounters increasing resistance near the mantle transition zone and lower mantle (Chen et al., 2004). Together, these observations show that subduction-zone stress fields are strongly depth dependent and cannot be inferred from plate convergence alone.

Stress in subduction zones also evolves through the seismic cycle. During the interseismic period, compressive stress accumulates at the shallow plate interface, whereas coseismic rupture and the postseismic response can rotate the stress field and modify the style and distribution of surrounding seismicity (Hardebeck, 2012, 2017; Herman and Govers, 2020). This behavior was clearly observed after the 2011 Mw 9.0 Tohoku-oki earthquake, when stress inversions indicated marked changes in stress orientation and the earthquake population shifted toward more normal-faulting events in the upper plate and forearc region (Hardebeck and Okada, 2018; Hasegawa et al., 2012; Yoshida et al., 2012). Changes were also observed at greater depth where seismicity in the double seismic zone beneath northeastern Japan responded strongly after the mainshock (Delbridge et al., 2017), and more recent work suggests that the Tohoku-oki earthquake perturbed slab stresses over a broad depth range, influencing intermediate- to deep-focus seismicity far from the rupture area (Gardonio et al., 2024). The temporal change of stress state in subduction zones further motivates the use of stress models tailored to active subduction settings.

To better characterize stress conditions in subduction zones, this thesis additionally employs a global stress model derived specifically for plate interfaces using earthquake focal mechanisms. The background tectonic stress field along global subduction zones is estimated using catalog-based stress inversion of earthquake focal mechanisms in the upper 50 km surrounding the plate interface. By focusing on seismically active portions of convergent margins, this approach directly samples the stress field acting within the shallow megathrust and adjacent forearc and intraslab environments. The resulting stress field is represented by the orientations of the principal stress axes and, for visualization, by the direction of maximum horizontal compression (S_{Hmax}) together with the associated faulting regime.

Fig. 2.7 illustrates the inferred stress field across global subduction margins. For completeness, we also show the global maps of principal stress-axis orientations (azimuth and plunge) for the background model in Fig. 2.8. Reverse faulting dominates most regions, consistent with compression driven by plate convergence, and S_{Hmax} orientations are generally trench-normal. However, significant spatial variability is observed both along strike and between different margins. Several subduction zones exhibit strike-slip, normal, or unclassified stress regimes, indicating departures from simple convergence-dominated stress states.

This heterogeneity reflects the influence of additional tectonic processes superimposed on plate-driven loading, including slab rollback, oblique convergence, variations in slab geometry and coupling, and upper-plate deformation. Regions such as Cascadia, Ryukyu, Hikurangi, and the New Hebrides display particularly complex stress patterns, highlighting that stress orientation and regime cannot be inferred from plate kinematics alone.

Importantly, stress orientations inferred from focal-mechanism inversions differ in some regions from those derived from smoothed global models such as the World Stress Map (described in Paper II). Differences arise from both methodological factors and depth sensitivity: catalog-based inversions preferentially sample the seismogenic portion of the lithosphere, whereas WSM integrates a broader range of near-surface stress indicators. As a result, the subduction-zone stress field resolved here is especially well suited for examining how transient stress perturbations project onto the background tectonic stress acting on active faults.

In the context of this thesis, the global subduction-zone stress model provides a physically relevant reference within which surface-loading–induced stress changes can be evaluated. The pronounced spatial heterogeneity observed along convergent margins underscores the importance of local stress conditions when assessing the sensitivity of seismicity to small external perturbations.

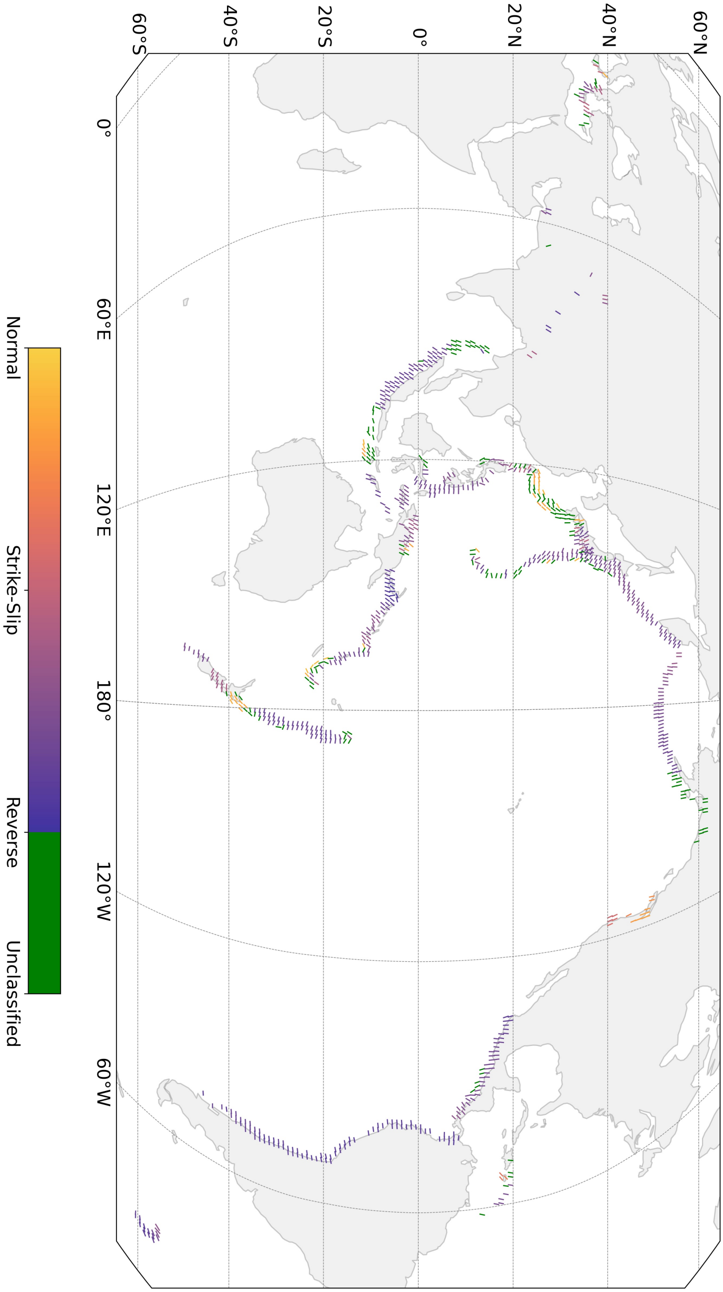

Fig. 2.7: *Background tectonic stress field along global subduction zones around plate interface inferred from focal-mechanism stress inversion. Stress orientation is shown by* S_{Hmax}*, and colors indicate faulting regime following Andersonian classification.*

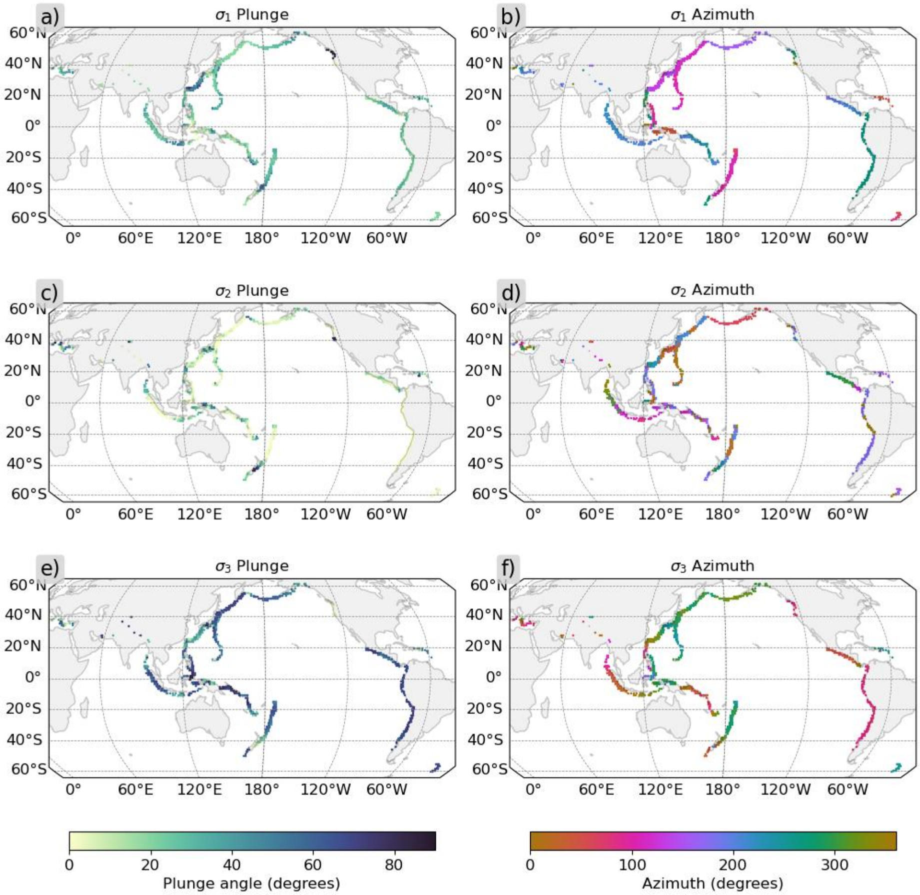

Fig. 2.8: *Principal stress-axis orientations for the background stress field. Each row shows the plunge (left) and azimuth (right) of (top)* σ_1*, (middle)* σ_2*, and (bottom)* σ_3 *across global subduction margins (upper 50 km around the Slab2 interface).*

Chapter 3

Surface loading as a source of stress variation

Surface loading represents one class of non-tectonic stress perturbations. More broadly, a range of non-tectonic processes, including surface loading (hydrological loading, atmospheric pressure variations, and non-tidal ocean mass redistribution), temperature-related thermoelastic effects, solid Earth and ocean tides driven by lunisolar forcing, polar motion, and post-glacial rebound, can modify the stress state of the crust. Although most non-tectonic stress perturbations are generally on the order of a few kPa (Bettinelli et al., 2008; Bollinger et al., 2007; Cai and Mouyen, 2024; Heki, 2003; Hsu et al., 2025, 2021; Johnson et al., 2017; Lu et al., 2018), they are not negligible, as they are comparable to stress changes known to influence earthquake timing (Freed, 2005). In addition, a growing body of observational and modeling work has shown that various geophysical phenomena are sensitive to variations in non-tectonic stress, including earthquakes (Craig et al., 2017), slow slip events (Liu et al., 2009; Lowry, 2006), tectonic tremor (Nakata et al., 2008), and volcanic activity (Kasahara, 2002). Some non-tectonic stress perturbations can be substantially larger, reaching tens of MPa in special settings, particularly during glacial isostatic adjustment in formerly glaciated regions and from pore-pressure changes associated with anthropogenic fluid injection, which affect the local stress field and may promote fault slip (Ellsworth, 2013; Moein et al., 2023; Steffen and Steffen, 2021). Within this broad range of forcing mechanisms, this thesis focuses on surface loading processes and their associated stress variations.

3.1 Surface loading processes

Surface loading refers to the redistribution of mass at or near the Earth's surface. As shown in Fig. 3.1, variations in continental water storage, atmospheric pressure, ocean bottom pressure, sediment transport and ice mass modify the distribution

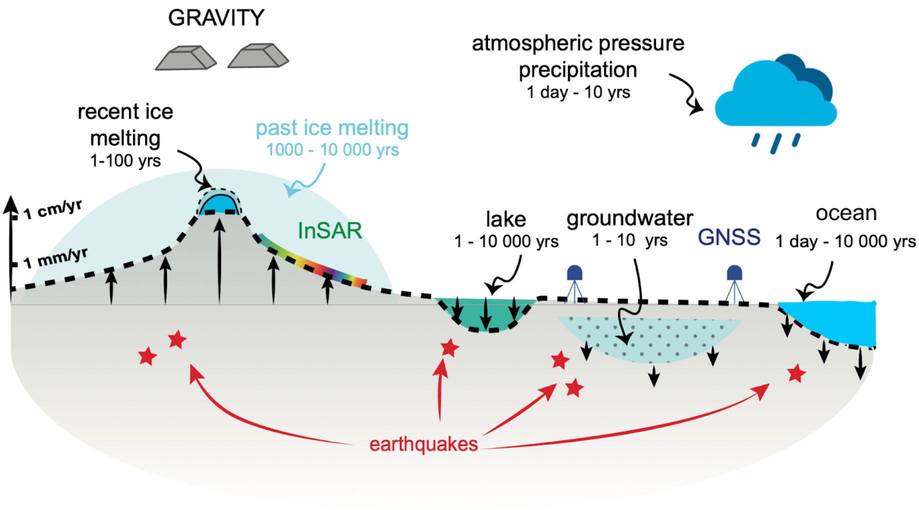

Fig. 3.1: *Sketch of (visco-) elastic climate-driven loadings and the commonly used observation techniques. Modified from Bürgmann et al. (2024).*

of surface mass and thereby perturb the stress state of the solid Earth.

Surface loading processes can be broadly categorized according to the source of mass variation. Hydrological loading arises from changes in terrestrial water storage, including precipitation, snow accumulation and melt, soil moisture, and groundwater variations. Atmospheric loading reflects spatiotemporal changes in surface air pressure associated with weather systems and seasonal circulation patterns. Non-tidal ocean loading results from variations in ocean bottom pressure driven by wind stress, ocean circulation, and large-scale climate variability. The Earth responds elastically to these loading sources. We note that glacial loading due to the growth and loss of land ice should be treated separately. While seasonal snow is part of the hydrological cycle, glacier and ice-sheet mass changes produce signals different from the seasonal pattern in regions affected by past or ongoing deglaciation. In the context of subduction settings, this is especially important in regions such as Alaska and western Canada, where contemporary ice loss is observed and present-day deformation may reflect not only the instantaneous elastic response to ongoing mass loss but also the longer-timescale legacy of deglaciation. Fig. 3.2 illustrates both elastic and viscoelastic responses. In this thesis, we focus on present-day elastic deformation and seasonal/cyclic stress variations.

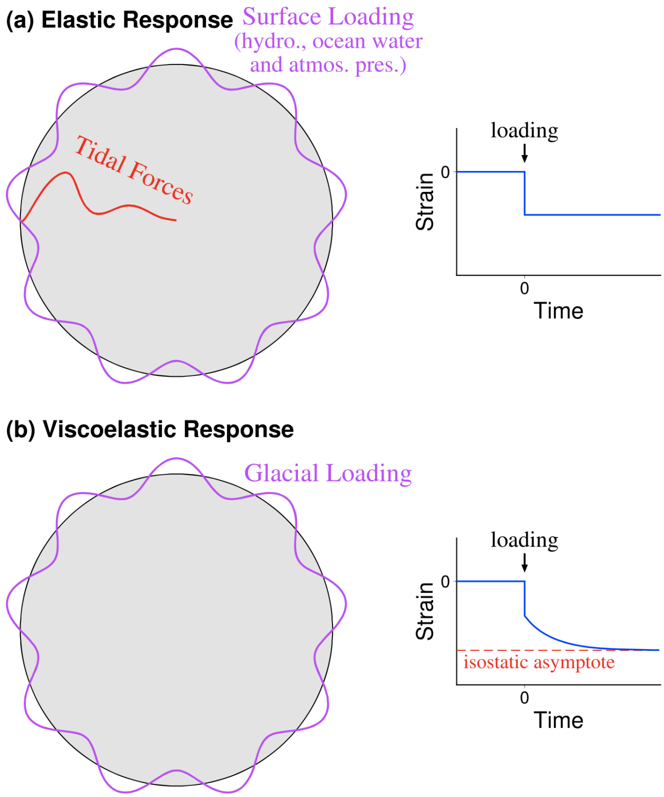

Fig. 3.2: *Sketch of loading forces and the Earth's elastic and viscoelastic responses. (a) Short-period hydrological, oceanic, atmospheric, and tidal loading; (b) glacial loading and the corresponding viscoelastic response. Reproduced from Lu et al. (2018).*

3.2 Surface loading observations

The mass redistribution of loading processes can be observed or inferred through its deformational, kinematic and gravitational effects (Farrell, 1972; Heki and Jin, 2023). Geodetic techniques such as GNSS and InSAR measure surface displacements associated with loading-induced deformation (Chanard et al., 2014; Xue et al., 2021; Zhao et al., 2016), while in situ observations and numerical models provide estimates of specific loading components (Mikolaj et al., 2016; Royer et al., 2021; Salstein et al., 2008). Satellite gravimetry, in contrast, provides an integrated measure of mass redistribution by observing variations in the Earth's gravity field (Chen et al., 2022; Tapley et al., 2004).

Surface loading signals can be constrained using a combination of observations and models (Chanard et al., 2018; Heki and Jin, 2023), each sensitive to different components of the Earth system. From a geophysical perspective, the aforementioned approaches offer complementary views of the physical processes. Model-based loading estimates often resolve individual sources of mass variation, whereas gravity-based observations capture the combined effect of multiple surface loads acting together. In this thesis, both perspectives are relevant for quantifying loading-induced stress variations.

3.2.1 Estimates of individual loading processes

Individual components of surface loading sources can be estimated based on observations and models. Hydrological loading can be estimated from land surface models like the Central Valley Hydrologic Model (CVHM, Faunt et al., 2016) and land data assimilation systems, such as the Global Land Data Assimilation System (GLDAS, Rodell et al., 2004), which provides fields of soil moisture, snow water equivalent, and evapotranspiration together with meteorological forcing such as precipitation. Atmospheric loading can be derived from global surface pressure fields from meteorological reanalyses such as ERA5, the fifth-generation atmospheric reanalysis produced by the European Centre for Medium-Range Weather Forecasts (ECMWF, Hersbach et al., 2020). Non-tidal ocean loading can be inferred from ocean circulation or state-estimate products such as the Ocean Model for Circulation and Tides (OMCT, Thomas, 2002) and Estimating the Circulation and Climate of the Ocean (ECCO, ECCO Consortium et al., 2021), which provide time-varying ocean bottom pressure fields. Long-term glacial and ice-sheet loading can be modeled using ice history reconstructions and glacial isostatic adjustment frameworks with viscoelastic Earth structure, for example, ICE-6G (Peltier et al., 2015).

Component-specific loading estimates provide detailed insight into the spatial and temporal structure of individual loading processes and allow their mechanical effects to be evaluated separately. They are particularly useful for isolating dominant contributors to loading-induced stress variations and for investigating the physical mechanisms linking specific surface processes to crustal deformation.

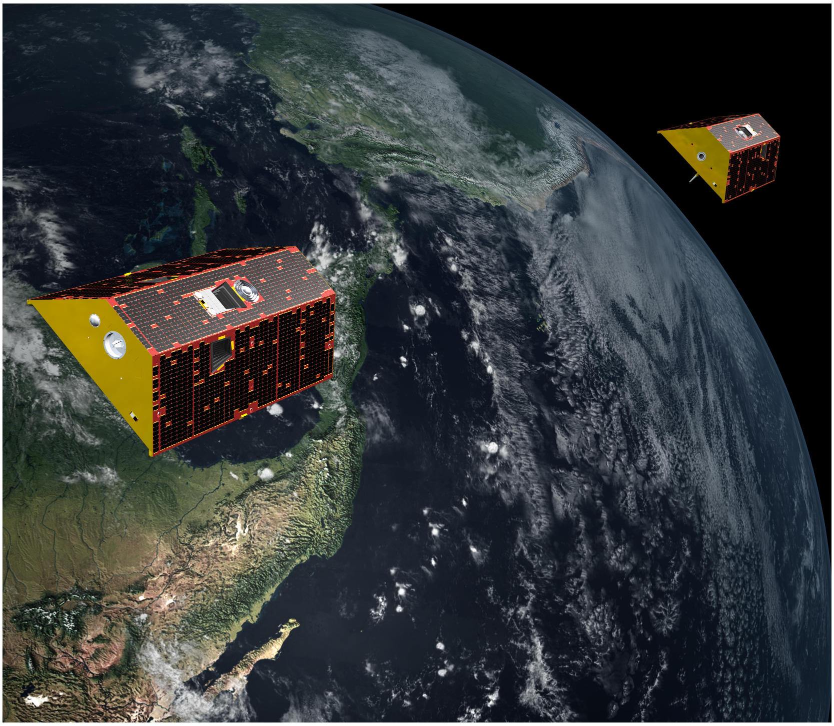

Fig. 3.3: *Illustration of the twin spacecraft of NASA and GFZ's GRACE-FO (Gravity Recovery and Climate Experiment Follow-On) mission, which monitors changes in Earth's mass distribution to track the evolution of the global water cycle. Credit: NASA/JPL-Caltech, https://www.jpl.nasa.gov/images/pia22440-grace-follow-on-satellites-artists-concept/*

3.2.2 GRACE and GRACE-FO satellite gravimetry

Satellite gravimetry offers a complementary and integrated approach to observing surface loading by directly measuring time-variable gravity associated with mass redistribution. The Gravity Recovery and Climate Experiment (GRACE) mission (Tapley et al., 2004) and its successor, GRACE Follow-On (GRACE-FO, Fig. 3.3) (Landerer et al., 2020), provide global observations of Earth's gravity field at monthly timescales, capturing mass changes associated with hydrology, ice loss, ocean dynamics, and atmospheric variability.

Both GRACE and GRACE-FO missions consist of pairs of satellites flying in tandem and measuring changes in their relative separation with micrometer precision using a microwave ranging system (Landerer and Cooley, 2021; Tapley et al., 2004). GRACE-FO additionally carried an experimental laser ranging interferometer with at least tenfold higher precision (Landerer and Cooley, 2021).

Variations in Earth's gravity field cause subtle accelerations of the leading and trailing satellites, allowing mass anomalies beneath the orbit to be inferred. After correcting for non-gravitational forces and background signals, these measurements provide gravity fields that reflect net surface mass redistribution.

Unlike component-specific models, GRACE-derived products observe the combined effect of multiple surface loading processes, providing a physically consistent measure of total mass change. This integrated perspective is particularly valuable in regions such as subduction zones, where multiple loading sources act simultaneously and ground-based observations are often sparse.

3.2.3 Global GRACE/GRACE-FO loading products

GRACE and GRACE-FO gravity solutions are distributed in several product forms that are widely used in geophysical applications. Level-2 products provide spherical harmonic representations of the time-variable gravity field, while Level-3 products offer gridded estimates of surface mass change, commonly expressed as equivalent water thickness in cm (EWT). These products are generated by multiple processing centers, such as GFZ, JPL, CSR, GFSC, allowing intercomparison and uncertainty assessment.

Two types of GRACE/GRACE-FO Level-3 products exist: spherical harmonic (SH) solutions (Boergens et al., 2019) and mass concentration (Mascon) solutions (Save et al., 2016; Watkins et al., 2015). Spherical harmonic products provide a compact global representation of gravity variations but require spatial filtering to suppress noise, which limits effective resolution. Mascon products estimate mass changes directly over predefined regions, improving spatial localization and signal recovery, particularly at regional scales. Fig. 3.4 gives example plots of both kinds of product. The SH product exhibits characteristic north-south striping and leakage along coastal regions, while the Mascon product shows a more blocky, patch-like spatial pattern. Both product types are available from multiple data centers and differ in their treatment of background models, filtering strategies, and leakage corrections (Landerer and Cooley, 2021).

In this thesis, the GRACE/GRACE-FO Level-3 SH products are used to quantify surface mass redistribution at seasonal to interannual timescales and to derive loading-induced stress perturbations relevant to subduction-zone seismicity. While GRACE/GRACE-FO products do not resolve individual faults or small-scale structures, they provide a robust and internally consistent measure of large-scale loading signals that can be projected onto tectonic stress fields and fault systems. The limitations associated with spatial resolution, temporal sampling, and signal separation are discussed in the following section.

3.2.4 Spatial and temporal resolution and limitations

Observations of surface loading are inherently limited by the spatial and temporal scales at which mass redistribution can be resolved. These limitations arise both

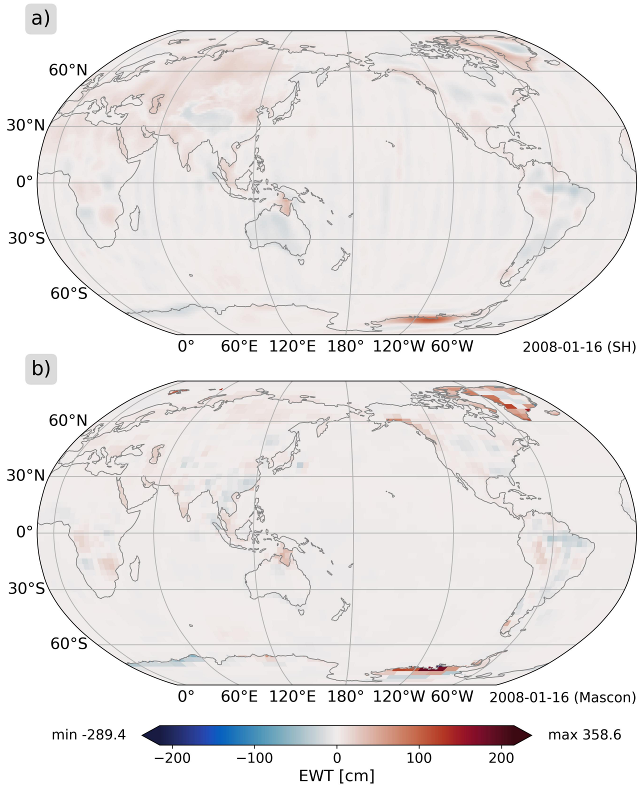

Fig. 3.4: *Global terrestrial water storage anomalies from GRACE RL06 products for an example month, January 2018, which is given as equivalent water thickness (EWT) in cm. (a) GFZ spherical harmonic (SH) solution. (b) JPL Mascon solution. Both are referenced to the 2002–2020 baseline.*

from the characteristics of the observing systems and from the physical nature of surface loading processes themselves. Understanding these constraints is essential for interpreting loading-induced stress variations and their potential influence on seismicity.

Satellite gravimetry from GRACE and GRACE-FO provides global coverage of time-variable mass redistribution but is restricted in spatial resolution, with effective wavelengths typically exceeding several hundred kilometers (Landerer et al., 2020; Landerer and Cooley, 2021). As a result, GRACE-derived loading products cannot resolve small-scale features or individual fault structures, and localized loading signals may be spatially smoothed or attenuated (Loomis et al., 2021). Temporal resolution is also limited, with most standard products provided at monthly intervals, precluding the direct and timely observation of short-period loading variations such as synoptic weather systems or individual storm events (Humphrey et al., 2016). However, these limitations are not critical for the surface loading processes considered in this thesis. Hydrological, atmospheric, and non-tidal oceanic mass variations generally exhibit long spatial wavelengths and evolve on seasonal to interannual timescales, particularly when integrated over continental or basin scales. Consequently, GRACE and GRACE-FO observations are well suited to capture coherent, large-scale stress perturbations in the lithosphere due to surface loading processes.

Complementary observations and models can partially mitigate these limitations. Geodetic techniques such as GNSS and InSAR resolve surface deformation at much finer spatial and temporal scales but their coverage is often uneven and restricted in oceanic, snowy, icy and other extreme environments. Component-specific models of hydrology, atmosphere, and ocean circulation provide higher temporal resolution but are subject to uncertainties in model parameters and processing strategy (Martens et al., 2020; Mikolaj et al., 2016). Each observational approach therefore samples different aspects of the surface loading system, and no single dataset fully captures all relevant scales.

In this thesis, we focus on loading-induced stress variations associated with large-scale, long-wavelength surface mass redistribution. While small-scale or short-period loading signals may influence localized deformation, the stress perturbations examined here are dominated by regional to continental-scale processes that are well represented by GRACE/GRACE-FO and global loading models. These considerations guide the interpretation of loading-induced stress fields and their projection onto tectonic stress states and fault systems.

3.3 Loading-induced stress variations

Observed surface mass redistribution does not directly provide stress products. Converting loads into stress variations requires a mechanical model of the Earth that links surface loads to deformation and stress. The mechanical response to surface loading depends on the forcing timescale and spatial scale: short-period and local loads primarily produce an elastic response in the crust and lithosphere, whereas long-term loading associated with ice sheets and post-glacial rebound can drive deformation that penetrates deeper into the Earth and requires viscoelastic relaxation in the mantle (Klemanna et al., 2014).

Two approaches are used to obtain loading-induced stress fields at the spatial and temporal scales relevant for tectonic applications. One pathway models individual loading components (e.g., hydrology, atmosphere, non-tidal ocean) from dedicated data products or reanalyses and then computes the elastic stresses they generate. A second way uses satellite gravimetry (GRACE/GRACE-FO) to observe the combined surface mass redistribution and subsequently models the elastic stress response. In this thesis, elastic loading stresses are obtained using both of the approaches. In Paper I, the database of Lu et al. (2018)

provides global non-tectonic loading stress variations derived using an elastic, compressible 1-D Earth structure (Gutenberg-Bullen A, Alterman et al., 1961) and component-specific forcing fields. In Paper II, stress tensors for global grids are computed from GRACE/GRACE-FO Level-3 products using the open-source toolkit LoadDef (Martens et al., 2019) with a spherically symmetric layered Earth model (PREM) (Dziewonski and Anderson, 1981; Guo et al., 2004).

3.3.1 Elastic response of the lithosphere

For the timescales emphasized here, loading-induced stress changes are modeled as the elastic responses of the Earth to surface mass redistribution (see Fig. 3.2). The loading-induced stress change at a given time, location, and depth is represented by a symmetric second-order tensor $\boldsymbol{T}$ with six independent components. Loading-induced-stress products are often provided in a spherical coordinate system r–θ–ϕ, where r is radial, θ is colatitude ($90° -$ latitude), and ϕ is longitude. We denote this tensor as $\boldsymbol{T}_{r\theta\phi}$.

$$\boldsymbol{T}_{r\theta\phi} = \begin{bmatrix} T_{rr} & T_{\theta r} & T_{\phi r} \\ T_{r\theta} & T_{\theta\theta} & T_{\phi\theta} \\ T_{r\phi} & T_{\theta\phi} & T_{\phi\phi} \end{bmatrix} \tag{3.1}$$

For applications that require resolving stresses locally, it is also convenient to work in a local geographic Cartesian frame, here taken as North–East–Down (NED). Using the local basis relations

$$\hat{\mathbf{N}} = -\hat{\boldsymbol{\theta}}, \qquad \hat{\mathbf{E}} = \hat{\boldsymbol{\phi}}, \qquad \hat{\mathbf{D}} = -\hat{\mathbf{r}}, \tag{3.2}$$

the tensor can be transformed from r–θ–ϕ to NED as

$$\boldsymbol{T}_{\text{NED}} = \begin{bmatrix} T_{NN} & T_{EN} & T_{DN} \\ T_{NE} & T_{EE} & T_{DE} \\ T_{ND} & T_{ED} & T_{DD} \end{bmatrix} = \begin{bmatrix} T_{\theta\theta} & -T_{\theta\phi} & T_{r\theta} \\ -T_{\theta\phi} & T_{\phi\phi} & -T_{r\phi} \\ T_{r\theta} & -T_{r\phi} & T_{rr} \end{bmatrix} \tag{3.3}$$

where $\boldsymbol{T}_{\text{NED}}$ is also symmetric. Throughout this thesis we adopt the convention that compressive normal stress is positive. When an input product uses the opposite convention, the sign is adjusted consistently prior to further calculations.

Because surface loading signals have long spatial wavelengths, the resulting elastic stress perturbations are typically smooth and spatially coherent over regional to continental scales (Fig. 3.5). At the same time, the stresses relevant to fault slip depend on how $\boldsymbol{T}$ is evaluated relative to fault geometry or the ambient tectonic stress state. The two projection strategies used in this thesis, resolving tractions on fault planes in one study and projecting onto principal tectonic stress directions in the other, are introduced in Chapter 4, while the present chapter establishes the physical basis for computing the loading-induced stress tensors that underlie both approaches.

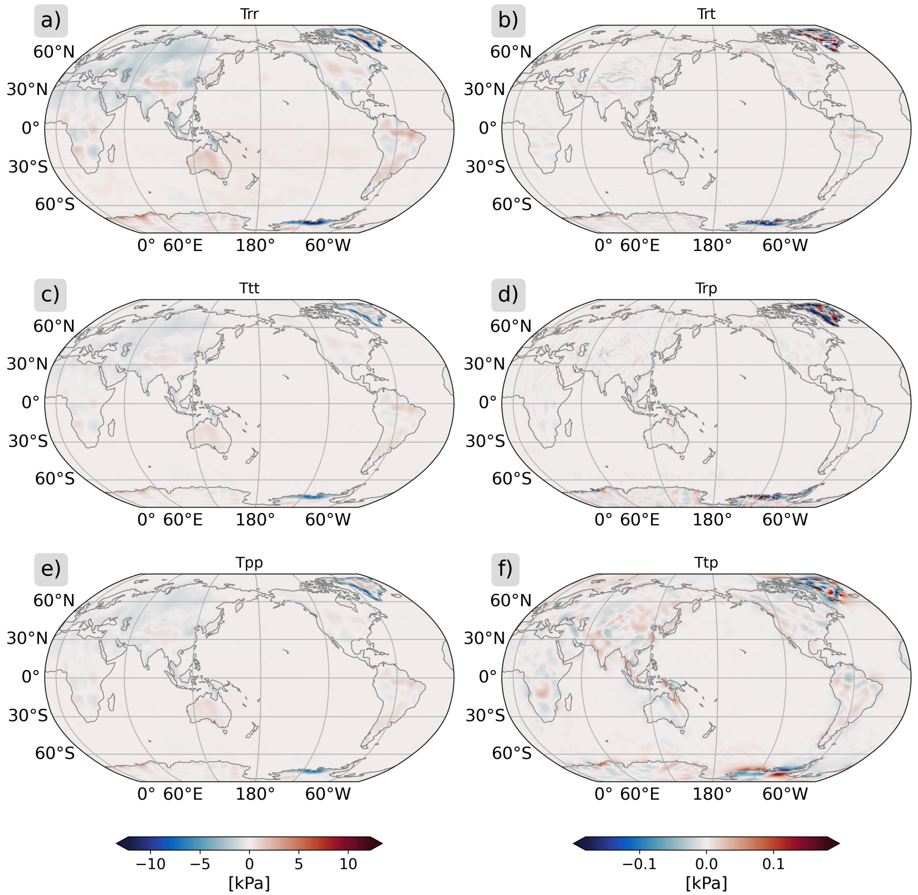

Fig. 3.5: *Global loading-induced stress components at 10 km depth for an example month derived from GRACE RL06 spherical harmonic solutions. The left column shows the diagonal tensor components (T_{rr}, T_{tt}, T_{pp}), and the right column shows the off-diagonal components (T_{rt}, T_{rp}, T_{tp}) in spherical coordinates. Stresses are expressed in kPa and plotted using separate symmetric color scales for diagonal and off-diagonal components to account for their different magnitudes.*

Chapter 4

Stress variations in a tectonic context

This chapter outlines how loading-induced stress tensors (Chapter 3) are evaluated in a tectonic setting relevant to earthquake occurrence in subduction environments. The two main papers motivating this thesis adopt two evaluation strategies, as summarized in Fig. 1.2. The first resolves loading-induced stresses onto the subduction interface to obtain normal and shear stress changes and the Coulomb failure stress change ΔCFF. The second evaluates loading-induced stress variations relative to the ambient tectonic stress field inferred from earthquakes by projecting the perturbations onto the principal stress directions. Both strategies start from the loading-induced stress changes, but differ in which tectonic information is used to contextualize it.

4.1 Conceptual frameworks for stress evaluation

Loading-induced stress variations are typically at a few kPa, but they are spatially coherent and temporally repeatable, making them suitable for testing hypotheses of stress modulation. But how to evaluate the mechanical relevance of those changes for subsurface structure and earthquake nucleation?

The approach used in Paper I is a *fault-plane-based* framework, in which $\boldsymbol{T}$ is resolved onto a specified fault plane to obtain changes in normal and shear traction and, optionally, Coulomb failure stress change ΔCFF (King et al., 1994). This framework is most direct when the relevant fault surface is known or can be approximated, as for shallow megathrust interfaces. The method used in Paper II is a *principal-axis-oriented* framework, in which $\boldsymbol{T}$ is evaluated relative to the orientations of the principal stress axes of the ambient tectonic stress field inferred from focal-mechanism stress inversion (Hardebeck and Michael, 2006). Rather than requiring a rupture surface, this approach assesses whether loading-induced stresses tend to reinforce or oppose the existing tectonic stress orientation. This is particularly useful where deformation is distributed across multiple fault populations or where fault geometry is uncertain, for example in forearc fault systems and intraslab seismicity at intermediate depths.

Both frameworks rely on simplifying assumptions that shape interpretation. For the fault-plane-based approach, the primary assumptions are that (i) the adopted fault geometry and slip direction provide an adequate representation of the mechanically relevant structure, and (ii) loading-induced stresses can be treated as small perturbations superimposed on a background tectonic stress state. Additional assumptions enter through the Coulomb formulation, including the choice of effective friction coefficient and pore-pressure effects (Cocco and Rice, 2002; King et al., 1994). As a result, absolute ΔCFF amplitudes can be sensitive to uncertainties in interface geometry, rake choice, and frictional parameters.

For the principal-axis-oriented approach, the key assumptions are that (i) focal mechanisms provide a representative sample of the stress field within the analyzed volume and time window, and (ii) the stress field can be approximated as homogeneous within each inversion cell (Hardebeck and Michael, 2006). Because stress inversions recover the stress sampled by seismic records, the inferred field may be biased toward the actively seismogenic portion of the lithosphere and may not fully capture aseismic or long-term stresses. Comparisons between loading-induced stress variations and inferred tectonic stress must also consider depth sensitivity: loading stresses are typically long-wavelength and smoothly varying with depth in 1-D Earth models, whereas the ambient tectonic stress field may vary with structural domain and depth.

Within these constraints, both frameworks provide useful and complementary ways to evaluate non-tectonic stress modulation. The following section introduces the fault-plane-based approach used in Paper I. We then describe the principal-axis-oriented approach used in Paper II.

4.2 Stress variations resolved on fault planes

A way to assess whether loading-induced stress perturbations may influence earthquakes is to resolve the loading-induced stress tensor $\boldsymbol{T}$ onto the fault plane and quantify the resulting changes in normal and shear traction. These traction changes can be combined into a Coulomb failure stress change (ΔCFF), which summarizes whether the perturbation would tend to promote or inhibit slip under an assumed frictional failure criterion. In subduction zones, this approach is particularly relevant for shallow interface earthquakes because the megathrust geometry can be approximated using global slab models such as Slab2 (Hayes et al., 2018).

Conceptually, the workflow consists of four steps: (1) express $\boldsymbol{T}$ in a local geographic reference frame, (2) define the fault-plane orientation from strike and dip, (3) compute traction changes and decompose them into normal and shear components, and (4) compute ΔCFF using an effective friction formulation.

In this thesis, $\boldsymbol{T}$ is available in spherical components $\boldsymbol{T}_{r\theta\phi}$ and is transformed locally into North–East–Down components $\boldsymbol{T}_{\text{NED}}$ (see details in Section 3.3). As shown in Fig. 4.1, fault orientation (strike and dip) is obtained from the plate interface geometry, and the rake direction is prescribed following megathrust kinematics.

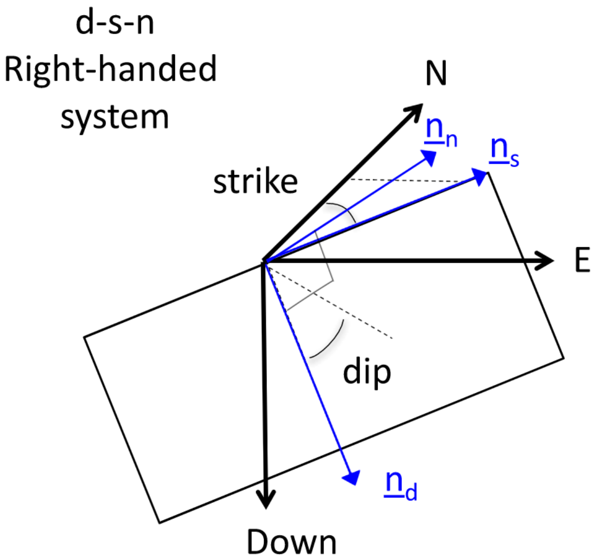

Fig. 4.1: *Fault coordinate system and the associated unit vectors (strike $\underline{\mathbf{n}}_{\mathbf{s}}$, dip $\underline{\mathbf{n}}_{\mathbf{d}}$, and normal $\underline{\mathbf{n}}_{\mathbf{n}}$). N, E, Down denote the geographical coordinate system North–East–Down. Reproduced from Espinoza (2024).*

Given a unit normal vector $\underline{\mathbf{n}}_{\mathbf{n}}$ for the fault plane, the traction vector acting on the plane is obtained as,

$$\Delta\mathbf{t} = \boldsymbol{T}_{\text{NED}}\,\underline{\mathbf{n}}_{\mathbf{n}}, \tag{4.1}$$

which can be decomposed into normal and shear components. The (signed) normal stress change is

$$\Delta\sigma_n = \Delta\mathbf{t}\cdot\underline{\mathbf{n}}_{\mathbf{n}}, \tag{4.2}$$

and the magnitude of the shear stress change is

$$\Delta\tau_a = \left\|\Delta\mathbf{t} - (\Delta\mathbf{t}\cdot\underline{\mathbf{n}}_{\mathbf{n}})\,\underline{\mathbf{n}}_{\mathbf{n}}\right\|. \tag{4.3}$$

To relate shear stress changes to slip, the traction is resolved onto the rake as

$$\begin{aligned}\Delta\tau &= \Delta\tau_a * \cos(rake_{stress} - rake_{fault}) \\ &= \Delta\tau_a * \cos(\arctan(\frac{\mathbf{\Delta t} \cdot \underline{\mathbf{n}}_{\mathbf{d}}}{\mathbf{\Delta t} \cdot \underline{\mathbf{n}}_{\mathbf{s}}}) - rake_{fault})\end{aligned} \tag{4.4}$$

The Coulomb failure stress change combines shear and normal stress changes into a scalar measure of whether the perturbation would tend to encourage ($\Delta CFF > 0$) or discourage ($\Delta CFF < 0$) fault slip. The definition is

$$\Delta CFF = \Delta\tau - \mu\left(\Delta\sigma_n - \Delta p\right), \tag{4.5}$$

where μ is the friction coefficient and Δp is the pore-pressure change. Because pore-pressure changes are generally not observed directly at the spatial scales considered here, it is common to adopt an effective friction coefficient μ' that absorbs pore-pressure effects (Cocco and Rice, 2002; King et al., 1994):

$$\Delta CFF = \Delta\tau - \mu'\,\Delta\sigma_n. \tag{4.6}$$

In this thesis, loading-induced ΔCFF is used as an interpretable metric for comparing the timing and polarity of loading-induced stress perturbations with variations in seismicity. We emphasize that ΔCFF is not a deterministic predictor of rupture, but a physically motivated measure of how small stress perturbations project onto a prescribed fault surface under simplified frictional assumptions. Its applicability is therefore strongest where fault geometry and slip direction are well constrained, and more limited in settings with distributed deformation or poorly defined rupture planes. These considerations motivate the complementary, geometry-independent framework introduced in the next section.

4.3 Stress variations resolved on ambient stress

In this framework, the tectonic context is represented by the orientations of the principal stress axes ($\sigma_1, \sigma_2, \sigma_3$) estimated from focal mechanisms. The loading-induced stress tensor $\boldsymbol{T}$ is then interpreted by projecting it onto these principal directions. Instead of evaluating slip tendency on a prescribed fault plane, this approach asks whether loading-induced stress variations act in the same sense as, or opposite to, the prevailing tectonic stress orientation and regime inferred from earthquakes.

Earthquake focal mechanisms provide fault orientation and slip information for individual events. When sufficient mechanisms are available within a region, they can be used to estimate a stress field that best explains the observed population (Hardebeck and Michael, 2006). In Paper II, the ambient stress field along global subduction zones is inferred using a damped stress inversion following Hardebeck and Michael (2006). The inversion results are expressed as the orientations of σ_1, σ_2, and σ_3 for each spatial cell included in the analysis.

At each location, the stress inversion provides the orientations of the three principal stress axes as azimuth and plunge, which define three unit vectors $\mathbf{e}_1$, $\mathbf{e}_2$, and $\mathbf{e}_3$ in a local geographic frame. The loading-induced tensor $\boldsymbol{T}$ is then projected onto each axis to quantify the normal stress change acting along that direction.

In our implementation, $\boldsymbol{T}$ is available as six independent components in the spherical r-θ-ϕ system, $\boldsymbol{T}_{r\theta\phi} = (T_{rr}, T_{\theta\theta}, T_{\phi\phi}, T_{r\theta}, T_{r\phi}, T_{\theta\phi})$ (Chapter 3). For projection, $\boldsymbol{T}_{r\theta\phi}$ is first transformed into the local North-East-Down tensor $\boldsymbol{T}_{\mathrm{NED}} = (T_{NN}, T_{EE}, T_{DD}, T_{NE}, T_{ND}, T_{ED})$ using the same rotation described in Section 3.3. The principal axes from the inversion are converted from azimuth and plunge into unit vectors in the NED frame,

$$\mathbf{e}(\mathrm{az}, \mathrm{pl}) = \begin{bmatrix} \mathbf{e_1} \\ \mathbf{e_2} \\ \mathbf{e_3} \end{bmatrix} = \begin{bmatrix} \cos(\mathrm{plunge})\cos(\mathrm{azimuth}) \\ \cos(\mathrm{plunge})\sin(\mathrm{azimuth}) \\ \sin(\mathrm{plunge}) \end{bmatrix}, \tag{4.7}$$

where azimuth is measured clockwise from north and plunge is measured downward from horizontal. The loading-induced normal stress change along each principal axis is computed as

$$\Delta\sigma_i = \mathbf{e}_i^{\mathsf{T}}\, \boldsymbol{T}_{\mathrm{NED}}\, \mathbf{e}_i, \qquad i \in \{1, 2, 3\}. \tag{4.8}$$

These projections are stored as time series $\Delta\sigma_1(t)$, $\Delta\sigma_2(t)$, and $\Delta\sigma_3(t)$ for each stress-inversion cell.

Two derived quantities are used to summarize the projected stress variations. First, the differential projection

$$\Delta\sigma_D = \Delta\sigma_1 - \Delta\sigma_3 \tag{4.9}$$

captures changes in compression along σ_1 relative to σ_3. Second, the mean normal stress change,

$$\Delta P = \frac{1}{3}\left(\Delta\sigma_1 + \Delta\sigma_2 + \Delta\sigma_3\right), \tag{4.10}$$

summarizes the isotropic part of the loading-induced stress perturbation in the principal-axis coordinate system.

For comparison with commonly used measures of loading-induced pressure in the lithosphere, we also compute the vertical stress change $\Delta\sigma_V$ by projecting onto the vertical unit vector $\mathbf{e}_v = [0, 0, 1]^{\mathsf{T}}$ in the NED frame. This corresponds to the Down component of $\boldsymbol{T}_{NED}$, and the radial component of $\boldsymbol{T}_{r\theta\phi}$.

This projection-based representation provides a compact way to interpret loading-induced stress variations relative to the dominant tectonic directions sampled by earthquakes. For example, in a compression-dominated margin where σ_1 is approximately horizontal and roughly trench-normal, positive $\Delta\sigma_1$ corresponds to increased compression along the dominant tectonic direction, while negative $\Delta\sigma_1$ corresponds to reduced compression. Because the principal axes are inferred from the local population of focal mechanisms, the projected stress time series provide a direct basis for comparing cyclic loading-induced stress variations with regional seismicity, without prescribing rupture planes.

The two stress evaluation frameworks described above are applied to subduction environments in complementary ways. In the fault-plane-based approach, loading-induced stress variations are resolved on a geometrically defined plate interface, using strike and dip information from Slab2 where an interface representation is appropriate for the target seismicity. In the principal-axis approach, the loading-induced stress variation is interpreted in a coordinate system defined by the ambient tectonic stress field inferred from focal mechanisms, which is especially useful where seismicity is distributed across multiple fault populations or spans broader depth ranges. With these stress metrics defined, the next chapter introduces how seismicity is treated as a response indicator and how earthquake catalogs, event selection, and statistical comparisons are used to evaluate whether cyclic loading-induced stress variations are associated with systematic modulation of earthquake occurrence.

Chapter 5

Seismicity as a response indicator

Modern global seismic monitoring is supported by seismic stations operated by many agencies worldwide. These observations feed into international services that curate and distribute earthquake catalogs, such as the International Seismological Centre (ISC), the United States Geological Survey (USGS), and the Global Centroid Moment Tensor project (GCMT). These catalogs are foundational for studies of earthquake occurrence, source properties, and spatiotemporal variations in seismicity rates.

A challenge for modulation studies is that earthquake catalogs mix multiple processes and timescales. In particular, catalogs contain both relatively isolated events and events that occur in clusters. Since this thesis evaluates whether small, cyclic stress perturbations are associated with systematic variations in earthquake occurrence, the way seismicity is represented (and filtered) is essential. Choices about catalog completeness, clustering, and declustering directly affect inferred rate changes, statistical significance, and physical interpretation.

5.1 Background seismicity and triggering concepts

Earthquake occurrence is often described as a combination of background activity and clustered activity (Kisslinger, 1996; Zaliapin and Ben-Zion, 2020). Background seismicity refers to events that are not obviously linked to a nearby prior earthquake in space and time, which reflects longer-term tectonic loading and the evolving stress state of the lithosphere (Dieterich, 1994; Zaliapin and Ben-Zion, 2020). Clustered seismicity includes aftershock sequences, foreshock activity, and earthquake swarms.

Aftershocks are clustered earthquakes promoted by the static and dynamic stress perturbations associated with the mainshock (Stein, 1999; Toda et al., 2012). Swarms are also clustered events, but they lack a single dominant mainshock. They can be associated with processes such as fluid pressure changes, slow slip, and volcanic or hydrothermal activity (Chen et al., 2012; Münchmeyer et al., 2025). In complex subduction settings, clustered activity can therefore reflect more than one mechanism. One complication is the occurrence of slow slip events (SSEs), which are episodes of transient fault slip that release strain more slowly than ordinary earthquakes and are typically identified geodetically rather than seismologically. Recent studies show that swarms may occur synchronously with SSEs (Dascher-Cousineau and Bürgmann, 2024; Kita et al., 2021; Münchmeyer et al., 2025). In such cases, part of the apparent seismic response to small external stress variations may reflect modulation of slow-slip-related swarm activity rather than only ordinary background seismicity.

Because clustered seismicity shapes both the apparent seismicity rate and how that rate is interpreted, it is important to identify and separate it in modulation studies. Aftershock sequences in particular can dominate short-term variability, which makes the weak periodic signal linked to non-tectonic stresses difficult to distinguish in the raw catalog. For this reason, this thesis focuses on an approximation of the background seismicity rate and uses declustering to reduce the influence of clearly clustered sequences, thereby narrowing the event population toward earthquakes that are less directly controlled by mainshock-driven triggering (Stiphout et al., 2012). At the same time, clustering is not necessarily irrelevant to modulation, since swarms and aftershocks may occur in conditions of elevated stress sensitivity (Dieterich, 1994; Llenos et al., 2009). Declustering is therefore best viewed as an operational filter that supports a specific goal, rather than a definitive separation between "modulated" and "non-modulated" earthquakes.

5.2 Earthquake catalog completeness

Seismicity rate analyses rely on the assumption that the earthquake catalog represents the underlying earthquake population in a consistent way through space and time. In practice, detection capability is limited by network geometry, noise conditions, processing strategies, and reporting practices. A standard way to account for these limits is to restrict analysis to events above the magnitude of completeness, M_c, and to treat M_c as a space- and time-dependent property of the catalog.

Magnitude of completeness

The magnitude of completeness M_c is commonly defined as the lowest magnitude above which earthquakes in a given space-time volume are assumed to be reliably detected and included in the catalog. For instance, $M_c = 1.0$ means that events with $M \geq 1.0$ are expected to be consistently recorded and reported, whereas smaller events may be missing. Applying an M_c threshold is important because events near the detection limit are sensitive to changes in network performance and reporting practice, which can introduce apparent rate variations that are not caused by changes in earthquake occurrence.

A common way to estimate M_c is to examine the frequency magnitude distribution (FMD) and identify the magnitude at which the observed distribution departs from the Gutenberg-Richter relation (Gutenberg and Richter, 1944). In its cumulative form, the Gutenberg-Richter model can be written as

$$\log_{10} N = a - b\,(m - M_c), \tag{5.1}$$

where N is the number of events with magnitude greater than or equal to m, a describes the overall productivity, and b quantifies the relative proportion of small and large earthquakes. In the observed FMD, incompleteness at low magnitudes causes a roll off from the linear Gutenberg-Richter trend, and M_c is often taken near the onset of this deviation. Fig. 5.1 illustrates this behavior for an example subduction-zone catalog.

In this thesis, M_c is estimated using two popular approaches. In Paper I, we use the Maximum Curvature (MAXC) method (Wiemer and Wyss, 2000), which identifies M_c at the magnitude where the non-cumulative FMD reaches its maximum (equivalently, the point of maximum curvature in the cumulative FMD). Operationally, this corresponds to the peak of the incremental magnitude histogram. In Paper II, we estimate M_c using a goodness-of-fit approach based on the Kolmogorov-Smirnov (KS) test, in which candidate cutoffs are evaluated by comparing the observed magnitude distribution above the cutoff with an expected Gutenberg-Richter model, and selecting the cutoff magnitude M_c that minimizes the KS distance.

Temporal and spatial variability

Completeness is rarely uniform across a global catalog. Spatial variability arises from differences in station coverage, offshore versus onshore settings, crustal structure, attenuation, and depth-dependent detectability. Temporal variability arises from changes in networks and processing, and also from transient conditions such as elevated noise or overlapping waveforms after large earthquakes. These effects can locally increase the effective detection threshold for days to months, depending on the region and the event sequence. As a result, M_c is best treated as region-specific and, when needed, time-dependent rather than fixed globally.

For global subduction zone analyses, this variability is especially important because margins differ strongly in earthquake behaviour and station density. A single global M_c can introduce systematic differences in sample size between regions and can bias comparisons among subduction zones. For that reason, M_c should be estimated for the specific spatial sampling used in the analysis (for example, per margin, per grid cell, or per depth range), and sensitivity tests with slightly different M_c choices are often informative.

Completeness choices directly affect inferred seismicity rates. A lower M_c increases event counts and improves statistical power, but it also increases sensitivity to catalog artifacts. A higher M_c reduces the risk of incompleteness bias,

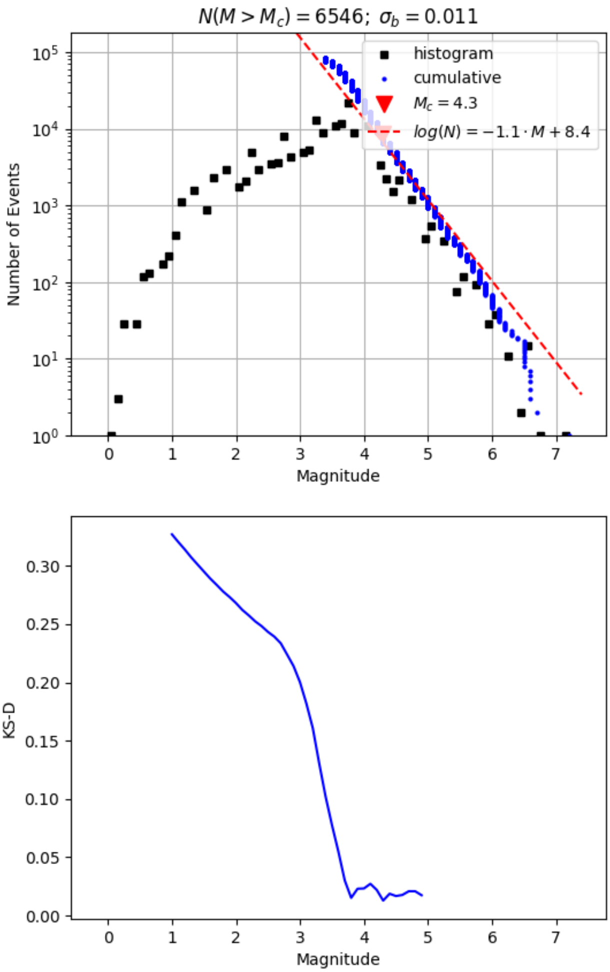

Fig. 5.1: *Example frequency-magnitude distribution (FMD) for earthquakes in the Aleutian subduction zone (2002–2024), shown for illustration. The dashed line indicates the Gutenberg-Richter trend above the estimated completeness magnitude ($M_c = 4.3$; KS-based estimate), with corresponding a and b parameters ($a = 8.4$, $b = 1.1$).*

but it reduces sample size and can weaken the ability to detect weak modulation signals. These trade-offs are central for studies of seasonal or interannual modulation, where the expected stress signals are small, and the inferred rate changes can be subtle.

5.3 Seismicity declustering

The declustering process separates an earthquake catalog into approximately independent events and dependent events associated with clusters. Declustering requires an operational definition of what constitutes a cluster, and that definition depends on the underlying model adopted by a given algorithm (Stiphout et al., 2012). There is therefore no universally best declustering method. Instead, different algorithms reflect different assumptions about triggering, characteristic space-time scales, and the extent to which earthquake sequences are connected through chains of interactions(Stiphout et al., 2012).

In the context of this thesis, declustering is to select an event set that better represents background seismicity. The motivation is that aftershock sequences are commonly interpreted as being triggered by stress changes associated with a mainshock, and their strong spatiotemporal clustering can dominate short-term rate variations. To focus on potential seismic modulation by surface loading-induced stress variations, we reduce the influence of clearly mainshock-triggered sequences to avoid conflating mainshock-driven triggering with externally imposed stress perturbations. Declustering operation systematically identifies earthquakes that are less directly controlled by nearby large events and are more suitable for background-rate analysis. At the same time, declustering outcomes depend on the chosen algorithm and parameters, so the resulting background catalog is method-dependent rather than unique.

Several declustering algorithms are widely used in earthquake science. In this section, we describe three approaches used in our work: (1) window methods, (2) linked-window methods, and (3) nearest-neighbor methods, which provide a metric-based way to classify dependent events. General background on these methods can be found in Stiphout et al. (2012) and Mignan and Woessner (2012). Implementations of the first two methods are available through the ZMAP toolkit (Wiemer, 2001), and code for the nearest-neighbor algorithm is made available by Goebel et al. (2019).

Gardner-Knopoff

The Gardner-Knopoff method is an example of the window method because it identifies dependent events using a space-time window that scales with the magnitude of a candidate mainshock (Gardner and Knopoff, 1974). For each event of magnitude M, subsequent events are classified as aftershocks if they occur within a prescribed time window $t(M)$ and distance window $d(M)$. The method is simple and computationally efficient, and it is widely used in hazard applications and exploratory analyses.

A key limitation is that the declustering outcome depends strongly on the chosen window parameters, which were originally calibrated for specific regions and time periods. Alternative parameterizations have therefore been proposed and are often adopted in practice, including the widely used Uhrhammer window formulation (Uhrhammer, 1986). Because window methods apply fixed magnitude-dependent thresholds, they can over-remove events in regions where aftershock sequences are long and spatially extended, and under-remove in regions where triggering scales differ from the assumed parameterization. Window methods also do not explicitly represent chain triggering in the sense that an aftershock of an aftershock is not treated differently from an event directly triggered by the largest shock, unless it falls within the window of the largest event.

Reasenberg

The Reasenberg algorithm builds clusters through a linked-window strategy (Reasenberg, 1985). Instead of using a single window around each mainshock, it links earthquakes into clusters when they fall within interaction zones defined in space and time. In this approach, a sequence can grow as new events are linked to previous ones, which allows the method to capture extended chains of clustering and to represent the fact that earthquake sequences often develop through multiple interactions rather than a single mainshock-aftershock pair.

In practice, the method requires choices of parameters controlling the spatial interaction distance (often related to magnitude scaling) and the temporal interaction duration (commonly guided by Omori-type decay of aftershock rates). Standard parameter sets have been proposed based on calibration in well-instrumented regions (Reasenberg, 1985), but performance can vary when applied to other tectonic settings, magnitude ranges, or catalog types. The method can also become sensitive to catalog completeness immediately after large events, when detection thresholds are temporarily elevated and the observed sequence may be incomplete, affecting how clusters are constructed.

Nearest-neighbor methods

Nearest-neighbor declustering provides an alternative perspective in which clustering is identified through proximity in a combined space-time-magnitude metric rather than through explicit windows (Zaliapin and Ben-Zion, 2013, 2020). Each earthquake is associated with its nearest predecessor in this metric, and the distribution of nearest-neighbor distances is used to separate clustered events from background-like events. This framework is attractive for large-scale analyses because it can adapt to regional differences in seismicity density and does not require predefined fixed windows.

In Paper II, we apply the nearest-neighbor approach to reduce the influence of aftershock clustering and to extract an approximately independent component of seismicity for comparison with loading-induced stress variations. The method uses rescaled temporal and spatial distances that depend on magnitude through Gutenberg-Richter scaling, and it can incorporate information about the spatial dimension of hypocenter distributions. A threshold nearest-neighbor distance is then used to classify events into dependent and independent groups. While this approach can be robust for heterogeneous catalogs, the classification depends on the chosen threshold and on parameters such as b and the dimension D, which may vary across regions and depth ranges.

Other approaches

Beyond the deterministic methods above, stochastic declustering approaches model seismicity as a superposition of background activity and triggered activity, often using epidemic-type models such as ETAS (Zhuang et al., 2002) or related model-independent stochastic declustering schemes (Marsan and Lengline, 2008). These methods can provide probabilistic cluster membership rather than hard assignments, but they introduce additional modeling assumptions and parameter estimation challenges. In this thesis, we focus on representative deterministic and metric-based declustering methods that are widely used and transparent. The resulting declustered catalogs are treated as operational representations of background seismicity, not as definitive separations between independent and clustered earthquake populations.

Chapter 6

Summary of included papers

6.1 Paper I: a regional study in Japan

In this paper, we investigate whether seasonal to interannual stress perturbations caused by surface mass redistribution can modulate earthquake occurrence in the Kamchatka–Kuril Islands–Japan subduction system. Using hydrological, atmospheric, and non-tidal ocean loading, we compute elastic stress tensors and resolve them onto the subduction interface defined by Slab2 to obtain loading-induced changes in normal and shear traction and the corresponding Coulomb failure stress change. We then compare the resulting monthly stress variations with regional seismicity from earthquake catalogs over the study period.

The analysis identifies a weak but statistically meaningful association between earthquake occurrence and loading-induced Coulomb stress changes, with the clearest signal in the shallow portions of the Japan and Kuril trenches. Although the inferred stress perturbations are small, typically a few kPa, they are temporally repeatable and spatially coherent, and their correlation with seismicity is consistent with the idea that parts of the interface are close to failure. The results also show that no single loading source dominates everywhere: the relative contributions of hydrology, atmosphere, and non-tidal ocean loading vary across the margin and through time, implying that treating surface loading as a combined, multi-source forcing is important when assessing potential seismicity modulation.

Contribution: I led this study from the initial design to the final manuscript. I carried out the data processing, coding, and statistical analyses, and I interpreted the results. I also prepared the figures and wrote the manuscript with inputs and feedback from the co-author.

6.2 Paper II: a global study across subduction zones

We evaluate how stress perturbation from cyclic surface loading influences the ambient tectonic stress field across global subduction zones. Surface mass redistribution is obtained from GRACE and GRACE-FO products. Elastic loading theory is applied with LoadDef and load Green's functions for a 1-D Earth structure to compute monthly stress tensors through the upper 50 km on a global 1° grid. Then we infer background principal stress orientations from focal mechanism catalogs using a damped stress inversion approach. The loading-induced stress variation at each location is then projected onto the inferred principal stress axes to form time series of stress changes along σ_1, σ_2, and σ_3, along with changes of differential stress, pressure, and vertical stress.

Using global observations of surface mass redistribution from GRACE/GRACE-FO together with focal-mechanism and seismicity catalogs, this study provides the first uniform, depth-resolved assessment of seismicity modulation by surface loading across global subduction zones. The projected stress fields exhibit coherent seasonal patterns, with peak-to-peak amplitudes of principal stress variations on the order of 1–4 kPa. The largest perturbations are typically associated with the principal stress axis oriented near vertical—most commonly $\Delta\sigma_3$ in reverse-faulting–dominated margins—reflecting the efficient transmission of surface loading into vertical stress changes. Although these stress amplitudes fall within the range previously suggested to influence earthquake timing, no uniform global modulation of seismicity is observed. Instead, the response depends on tectonic regime and region-specific conditions. Normal-faulting-dominated regions show the clearest sensitivity, with seismicity rates varying by up to 10% per kPa, whereas reverse-faulting regions exhibit little systematic modulation and largely dampen the aggregated global signal. At the scale of individual subduction zones, responses are heterogeneous: some subduction systems display seismicity changes consistent with loading-induced stress relaxation, while others show opposite or statistically insignificant trends. Overall, the results demonstrate that surface-loading–induced stress perturbations provide physically meaningful constraints on fault sensitivity and ambient stress state, but their seismic expression is strongly governed by tectonic setting, fault geometry, and stress heterogeneity, underscoring the importance of regionally focused analyses within a global framework.

Contribution: I led this study from conceptualization to manuscript. I was responsible for the data processing, implementation of the HPC computational workflow, coding, stress and seismicity analyses, and interpretation of the results. I also produced the visualizations and wrote the manuscript with inputs and feedback from the co-authors.

6.3 Paper III in context: an attempt at geodetic-seismology

In this paper, we develop and evaluate an automated framework for detecting S-wave arrivals and quantifying ground motion parameters from high-rate ($\geq$1 Hz) GNSS velocity time series. Although high-rate GNSS has demonstrated its capability to capture dynamic ground displacement during large earthquakes (Mw $\geq$ 6.0), robust and automated phase detection in comparatively noisy geodetic data has limited its systematic integration into earthquake monitoring and early warning (EEW) systems. To address this, we introduce a sliding-window–based detection algorithm specifically designed for GNSS velocity records, which identifies S-wave arrivals and extracts peak shaking amplitude and duration without requiring station-specific frequency-domain pre-filtering. The method is implemented in an open-source Python toolbox, GNSS S-wave Picker (GSWPicker), enabling automated, large-scale seismo-geodetic analysis.

The algorithm is tested using two major earthquakes: the 2016 Mw 6.5 Norcia event in Italy and the 2023 Mw 7.7 Kahramanmaraş–Gaziantep earthquake in Türkiye. GNSS-derived S-wave arrival times are validated against strong-motion–based reference arrivals derived from nearby P-wave picks. Across epicentral distances up to approximately 500 km, the method achieves root mean square errors of 1.8 s for the Norcia event and 3.8 s for the Kahramanmaraş–Gaziantep event, within the uncertainty range associated with reference phase picking and station collocation offsets. In addition, GNSS-derived shaking durations reach up to 90 s and 200 s for the two events, respectively, demonstrating that high-rate GNSS captures prolonged strong ground motion over regional scales.

Analysis of P-to-S travel-time delays indicates that existing high-rate GNSS networks could provide actionable warning times for population centers located tens of kilometers from the epicenter, highlighting their potential contribution to EEW systems. Overall, this study demonstrates that high-rate GNSS velocity data can reliably complement seismic strong-motion sensors for rapid ground motion characterization. By enabling automated extraction of S-wave arrivals and shaking parameters from geodetic time series, the developed framework facilitates the integration of GNSS into operational seismo-geodetic monitoring and strengthens the observational basis for earthquake early warning applications.

Contribution: This paper was developed as a collaborative study. My main contributions were to the seismic validation of the GNSS-based detections, the visualization of the results, and parts of the manuscript writing and revision.

Chapter 7

Concluding remarks and outlook

This thesis contributes to an evolving perspective in earthquake triggering theory that faults operate within a multiscale stress environment in which tectonic loading is modulated by smaller, externally imposed perturbations. While climate-driven surface loading induces small stress variations typically on the order of a few kPa, the results demonstrate that these perturbations are spatially coherent, cyclic, and physically quantifiable. In tectonic environments where faults are critically stressed, such perturbations may influence the timing of failure without altering the overall tectonic driving mechanism. More broadly, surface loading can serve not only as a potential trigger but also as a diagnostic probe of subsurface stress state and fault sensitivity. Surface loading, therefore, acts as a controlled, recurrent stress experiment imposed on the lithosphere, revealing where and under what conditions faults appear responsive to small perturbations.

The results in the attached papers show that the seismic expression of surface-loading stress perturbations is real but variable. The regional megathrust study in Paper I finds a modest yet statistically significant correlation between background seismicity and multi-source loading-induced Coulomb stress variations of a few kPa, with the clearest signal in the shallow southern segment near Hokkaido. It also shows that the dominant loading contribution varies across space, and it is meaningful to study the combined effect of multiple loading sources. The global analysis in Paper II demonstrates that loading-induced stress perturbations display seasonal patterns of kPa-level amplitude across subduction zones, but that their relationship to earthquake occurrence is not uniform. The response depends on faulting style and region-specific tectonic conditions, with some regions showing measurable modulation and others showing weak or opposite trends. Together, these results support the interpretation that surface loading provides physically meaningful constraints on fault sensitivity in subduction systems, while also underscoring that heterogeneity in stress state, structure, and deformation style controls how such perturbations are expressed in seismicity.

The global, depth-resolved stress products generated in this thesis provide a quantitative framework for evaluating where climate-driven stresses are most relevant. Under ongoing climate change, hydrological extremes and cryospheric mass loss are projected to intensify. Although long-term tectonic processes dominate seismic hazard, increasing surface mass redistribution may locally amplify stress modulation effects. Quantifying fault sensitivity to such perturbations therefore contributes to a more physically informed understanding of seismic risk under evolving environmental conditions.

Methodologically, this thesis highlights the importance of integrating environmental and tectonic stresses. By constructing a depth-resolved tectonic stress reference and systematically projecting environmental stress perturbations onto that reference, this work enables direct comparison of magnitudes, orientations, and relative importance across depth and regions. Moreover, the comparison between fault-plane-based and principal-axis-oriented approaches illustrates the trade-offs inherent in stress modeling strategies. The former provides physically intuitive measures, while the latter approach is more general and applicable to deeper or geometrically complex or unclear regions.

Limitations

This work has several limitations related to both modelling and data processing. One concerns the depth propagation of loading-induced stress perturbations. Elastic theory predicts that long-wavelength surface loads can generate stress changes at depth, but their coherence and mechanical relevance likely decrease with increasing depth and structural complexity. In this thesis, stress is resolved within the upper 50 km in order to focus on the subduction interface, so the full depth range of subduction systems is not captured. The current framework also assumes a predominantly elastic Earth response. In reality, viscoelastic relaxation, poroelastic effects, and time-dependent fault-zone processes may also modify how stresses are transmitted. In addition, the seismicity analysis depends on the declustering procedure, and ordinary background earthquakes in the declustered catalog are not explicitly separated from remaining seismicity associated with SSEs, tremor, or swarms.

Subduction zones also exhibit strong spatial heterogeneity in stress orientation and faulting regime. Forearcs, double seismic zones, slab bending, slab rollback, and upper-plate deformation all contribute to complex stress patterns. In such environments, small loading-induced stress variations may interact with the local stress field in ways that are not captured by spatially averaged models. The tectonic stress field derived from focal-mechanism inversion represents an average state over sampled grid cells. Local deviations from this average may affect how loading-induced stress changes are resolved on individual structures. Future work should therefore examine the scale dependence of stress orientation and the robustness of stress inversion in regions with sparse seismicity.

GRACE and GRACE-FO provide valuable constraints on large-scale mass redistribution, but their spatial and temporal resolution is limited. As a result, small-scale loading variations, especially near coastlines, may be underrepresented. Independent geodetic observations such as GNSS and InSAR provide complementary information on surface deformation and can help refine stress estimates at regional scales. Integrating these datasets is not straightforward, however. GNSS offers high temporal resolution but sparse spatial coverage. InSAR provides dense spatial sampling, but its temporal continuity is often more limited and its performance can be reduced in vegetated areas and over water. Combining these observations with satellite gravimetry in a physically consistent way remains both a methodological challenge and an opportunity to improve stress modelling.

Future directions

A natural extension of this work is to investigate not only instantaneous stress perturbations but also accumulated stress duration and stressing history. Examining how the duration and phase of loading cycles relate to earthquake occurrence may provide insight into time-dependent fault sensitivity. Expanding the stress budget to include additional forcing mechanisms, such as tidal stresses, thermoelastic effects, and present-day glacial loading, would enable a more complete assessment of environmental contributions to fault stability and may clarify whether different stress sources interact constructively or destructively in modulating seismicity. The methods developed here can also be applied to other tectonic environments, including continental strike-slip systems and rift zones, to evaluate whether stress modulation sensitivity varies systematically with tectonic regime.

Future satellite missions and improved processing strategies will enhance constraints on surface mass redistribution. Higher-resolution gravity solutions, longer time series, and improved treatment of leakage and filtering effects will refine stress estimates, while continued integration of GRACE/-FO with GNSS and InSAR observations will reduce uncertainty in deformation and stress modeling, particularly at regional scales. Advances in Earth structure models, including improved constraints on lithospheric rheology, will further improve stress-transfer calculations, and incorporating three-dimensional structural heterogeneity may reveal departures from the simplified elastic response assumed here. Coupling stress modeling with statistical earthquake triggering frameworks and physics-based simulations may further clarify the mechanisms by which small stress perturbations influence failure timing. Ultimately, combining environmental loading, tectonic stress inversion, geodetic deformation, and seismic response within a unified modeling framework offers a pathway toward a deeper understanding of lithospheric dynamics under ongoing climate variability.

Concluding perspective

This thesis demonstrates that climate-driven surface loading can be quantified globally, contextualized within a depth-resolved tectonic stress field, and evaluated against seismicity across subduction zones. While environmental stresses are small, their cyclic and externally constrained nature provides a powerful tool for interrogating subsurface stress conditions. By treating climate variability as a physically defined stress experiment imposed on the lithosphere, this work reframes surface loading from a secondary perturbation into a diagnostic probe of fault sensitivity. Continued refinement of observational constraints, stress modeling strategies, and integrative approaches will further clarify how environmental and tectonic processes interact within Earth's dynamic system.

References

Allen, R. M., P. Gasparini, O. Kamigaichi, and M. Bose (2009). The status of earthquake early warning around the world: An introductory overview. *Seismological research letters*, **80**(5), 682–693. DOI: 10.1785/gssrl.80.5.682.

Allen, R. M. and D. Melgar (2019). Earthquake early warning: Advances, scientific challenges, and societal needs. *Annual Review of Earth and Planetary Sciences*, **47**, 361–388. DOI: https://doi.org/10.1146/annurev-earth-053018-060457.

Alterman, Z., H. Jarosch, and C. Pekeris (1961). Propagation of Rayleigh waves in the Earth. *Geophysical Journal International*, **4**(Supplement_1), 219–241. DOI: https://doi.org/10.1111/j.1365-246X.1961.tb06815.x.

Bartlow, N. M., D. A. Lockner, and N. M. Beeler (2012). Laboratory triggering of stick-slip events by oscillatory loading in the presence of pore fluid with implications for physics of tectonic tremor. *Journal of Geophysical Research: Solid Earth*, **117**(B11). DOI: https://doi.org/10.1029/2012JB009452.

Beeler, N. and D. Lockner (2003). Why earthquakes correlate weakly with the solid Earth tides: Effects of periodic stress on the rate and probability of earthquake occurrence. *Journal of Geophysical Research: Solid Earth*, **108**(B8). DOI: https://doi.org/10.1029/2001JB001518.

Benetatos, C., A. Kiratzi, C. Papazachos, and G. Karakaisis (2004). Focal mechanisms of shallow and intermediate depth earthquakes along the Hellenic Arc. *Journal of Geodynamics*, **37**(2), 253–296. DOI: https://doi.org/10.1016/j.jog.2004.02.002.

Bettinelli, P., J.-P. Avouac, M. Flouzat, L. Bollinger, G. Ramillien, S. Rajaure, and S. Sapkota (2008). Seasonal variations of seismicity and geodetic strain in the Himalaya induced by surface hydrology. *Earth and Planetary Science Letters*, **266**(3-4), 332–344. DOI: https://doi.org/10.1016/j.epsl.2007.11.021.

Bilek, S. L. and T. Lay (2018). Subduction zone megathrust earthquakes. *Geosphere*, **14**(4), 1468–1500. DOI: https://doi.org/10.1130/GES01608.1.

Bloch, W., B. Schurr, J. Kummerow, P. Salazar, and S. A. Shapiro (2018). From slab coupling to slab pull: Stress segmentation in the subducting Nazca plate. *Geophysical Research Letters*, **45**(11), 5407–5416. DOI: http://dx.doi.org/10.1029/2018GL078793.

Boergens, E., H. Dobslaw, and R. Dill (2019). GFZ GravIS RL06 continental water storage anomalies. DOI: https://doi.org/10.5880/GFZ.GRAVIS_06_L3_TWS.

Bohnhoff, M., H.-P. Harjes, and T. Meier (2005). Deformation and stress regimes in the Hellenic subduction zone from focal mechanisms. *Journal of Seismology*, **9**(3), 341–366. DOI: https://doi.org/10.1007/s10950-005-8720-5.

Bollinger, L., F. Perrier, J.-P. Avouac, S. Sapkota, U. Gautam, and D. Tiwari (2007). Seasonal modulation of seismicity in the Himalaya of Nepal. *Geophysical Research Letters*, **34**(8). DOI: 10.1029/2006GL029192.

Bürgmann, R., K. Chanard, and Y. Fu (2024). "Chapter 14 - Climate- and weather-driven solid Earth deformation and seismicity". *GNSS Monitoring of the Terrestrial Environment, Chapter 14*. Elsevier, pp. 257–285. ISBN: 978-0-323-95507-2. DOI: https://doi.org/10.1016/B978-0-323-95507-2.00011-6.

Burkert, W. (1985). *Greek religion*. Harvard University Press, p. 137. ISBN: 0-674-36281-0.

Cai, L. (2015). The hermeneutics of omens: The bankruptcy of moral cosmology in Western Han China (206 BCE–8 CE). *Journal of the Royal Asiatic Society*, **25**(3), 439–459. DOI: doi:10.1017/S1356186315000048.

Cai, Yiting, Roland Bürgmann, Eva Boergens, Maxime Mouyen, Kristel Chanard, and Karine Le Bail (2026). Global modulation of stress and seismicity in subduction interfaces by surface loads. *Journal of Geophysical Research: Solid Earth*. Submitted.

Cai, Yiting and Maxime Mouyen (2024). Loading-induced stress variation on active faults and seismicity modulation in the Kuril Islands-Japan region. *Earth and Planetary Science Letters*, **643**, 118904. DOI: https://doi.org/10.1016/j.epsl.2024.118904.

Cammarano, F., S. Goes, P. Vacher, and D. Giardini (2003). Inferring upper-mantle temperatures from seismic velocities. *Physics of the Earth and Planetary Interiors*, **138**(3-4), 197–222. DOI: https://doi.org/10.1016/S0031-9201(03)00156-0.

Chanard, K., J. Avouac, G. Ramillien, and J. Genrich (2014). Modeling deformation induced by seasonal variations of continental water in the Himalaya region: Sensitivity to Earth elastic structure. *Journal of Geophysical Research: Solid Earth*, **119**(6), 5097–5113. DOI: https://doi.org/10.1002/2013JB010451.

Chanard, K., L. Fleitout, E. Calais, P. Rebischung, and J.-P. Avouac (2018). Toward a global horizontal and vertical elastic load deformation model derived from GRACE and GNSS station position time series. *Journal of Geophysical Research: Solid Earth*, **123**(4), 3225–3237. DOI: https://doi.org/10.1002/2017JB015245.

Chen, P.-F., C. R. Bina, and E. A. Okal (2004). A global survey of stress orientations in subducting slabs as revealed by intermediate-depth earthquakes. *Geophysical Journal International*, **159**(2), 721–733. DOI: https://doi.org/10.1111/j.1365-246X.2004.02450.x.

Chen, J., A. Cazenave, C. Dahle, W. Llovel, I. Panet, J. Pfeffer, and L. Moreira (2022). Applications and challenges of GRACE and GRACE follow-on satellite gravimetry. *Surveys in Geophysics*, **43**(1), 305–345. DOI: https://doi.org/10.1007/s10712-021-09685-x.

Chen, K. H. and R. Bürgmann (2017). Creeping faults: Good news, bad news? *Reviews of Geophysics*, **55**(2), 282–286. DOI: https://doi.org/10.1002/2017RG000565.

Chen, X., P. Shearer, and R. Abercrombie (2012). Spatial migration of earthquakes within seismic clusters in Southern California: Evidence for fluid diffusion. *Journal of Geophysical Research: Solid Earth*, **117**(B4). DOI: https://doi.org/10.1029/2011JB008973.

Coburn, A. and R. Spence (2003). *Earthquake protection*. John Wiley & Sons. ISBN: 978-0-470-85517-1.

Cocco, M. and J. R. Rice (2002). Pore pressure and poroelasticity effects in Coulomb stress analysis of earthquake interactions. *Journal of Geophysical Research: Solid Earth*, **107**(B2), ESE–2. DOI: 10.1029/2000JB000138.

Colledge, M., J. Aubry, K. Chanard, F. Pétrélis, C. Duverger, L. Bollinger, and A. Schubnel (2023). Susceptibility of microseismic triggering to small sinusoidal stress perturbations at the laboratory scale. *Journal of Geophysical Research: Solid Earth*, **128**(4), e2022JB025583. DOI: https://doi.org/10.1029/2022JB025583.

Craig, T. J., K. Chanard, and E. Calais (2017). Hydrologically-driven crustal stresses and seismicity in the New Madrid Seismic Zone. *Nature communications*, **8**(1), 2143. DOI: 10.1038/s41467-017-01696-w.

Cremen, G. and C. Galasso (2020). Earthquake early warning: Recent advances and perspectives. *Earth-Science Reviews*, **205**, 103184. DOI: `https://doi.org/10.1016/j.earscirev.2020.103184`.

Dascher-Cousineau, K. and R. Bürgmann (2024). Global subduction slow slip events and associated earthquakes. *Science Advances*, **10**(35), eado2191. DOI: `https://doi.org/10.1126/sciadv.ado2191`.

Day, R. W. (2012). *Geotechnical earthquake engineering handbook: with the 2012 International building code*. McGraw-Hill Education. ISBN: 978-0071792387.

Delbridge, B. G., S. Kita, N. Uchida, C. W. Johnson, T. Matsuzawa, and R. Bürgmann (2017). Temporal variation of intermediate-depth earthquakes around the time of the M9. 0 Tohoku-oki earthquake. *Geophysical Research Letters*, **44**(8), 3580–3590. DOI: `http://dx.doi.org/10.1002/2017GL072876`.

Dieterich, J. (1994). A constitutive law for rate of earthquake production and its application to earthquake clustering. *Journal of Geophysical Research: Solid Earth*, **99**(B2), 2601–2618. DOI: `https://doi.org/10.1029%2F93JB02581`.

Dieterich, J. H. (1979). Modeling of rock friction: 1. Experimental results and constitutive equations. *Journal of Geophysical Research: Solid Earth*, **84**(B5), 2161–2168. DOI: `https://doi.org/10.1029/JB084iB05p02161`.

Dixon, T. H. and J. C. Moore (2007). *The seismogenic zone of subduction thrust faults*. Columbia University Press. DOI: `https://doi.org/10.1017/S0016756808004834`.

Duarte, J. C. and W. P. Schellart (2016). *Introduction to plate boundaries and natural hazards*. Wiley Online Library. Chap. 1, p. 5. DOI: `https://doi.org/10.1002/9781119054146.ch1`.

Dziewonski, A. M. and D. L. Anderson (1981). Preliminary reference Earth model. *Physics of the Earth and Planetary Interiors*, **25**(4), 297–356. ISSN: 0031-9201. DOI: `https://doi.org/10.1016/0031-9201(81)90046-7`. URL: `https://www.sciencedirect.com/science/article/pii/0031920181900467`.

ECCO Consortium, I. Fukumori, O. Wang, I. Fenty, G. Forget, P. Heimbach, and R. M. Ponte (Feb. 2021). *Synopsis of the ECCO Central Production Global Ocean and Sea-Ice State Estimate, Version 4 Release 4*. Version 4 Release 4. DOI: `10.5281/zenodo.4533349`.

Ellsworth, W. L. (2013). Injection-induced earthquakes. *science*, **341**(6142), 1225942. DOI: `https://doi.org/10.1126/science.1225942`.

Espinoza, D. N. (2024). *Introduction to Energy Geomechanics*. URL: `https://dnicolasespinoza.github.io/node2.html`.

Farrell, W. (1972). Deformation of the Earth by surface loads. *Reviews of Geophysics*, **10**(3), 761–797. DOI: `https://doi.org/10.1029/RG010i003p00761`.

Faunt, C. C., M. Sneed, J. Traum, and J. T. Brandt (2016). Water availability and land subsidence in the Central Valley, California, USA. *Hydrogeology Journal*, **24**(3), 675–684. DOI: `https://doi.org/10.1007/s10040-015-1339-x`.

Ferrand, T. P., N. Hilairet, S. Incel, D. Deldicque, L. Labrousse, J. Gasc, J. Renner, Y. Wang, H. W. Green II, and A. Schubnel (2017). Dehydration-driven stress transfer triggers intermediate-depth earthquakes. *Nature communications*, **8**(1), 15247. DOI: `https://doi.org/10.1038/ncomms15247`.

Florez, M. and G. Prieto (2019). Controlling factors of seismicity and geometry in double seismic zones. *Geophysical Research Letters*, **46**(8), 4174–4181. DOI: `https://doi.org/10.1029/2018GL081168`.

Freed, A. M. (2005). Earthquake triggering by static, dynamic, and postseismic stress transfer. *Annu. Rev. Earth Planet. Sci.*, **33**(1), 335–367. DOI: `10.1146/annurev.earth.33.092203.122505`.

Gao, S. S., P. G. Silver, A. T. Linde, and I. S. Sacks (2000). Annual modulation of triggered seismicity following the 1992 Landers earthquake in California. *Nature*, **406**(6795), 500–504. DOI: `https://doi.org/10.1038/35020045`.

Gardner, J. and L. Knopoff (1974). Is the sequence of earthquakes in Southern California, with aftershocks removed, Poissonian? *Bulletin of the seismological society of America*, **64**(5), 1363–1367. DOI: `10.1785/BSSA0640051363`.

Gardonio, B., D. Marsan, T. Bodin, A. Socquet, S. Durand, M. Radiguet, Y. Ricard, and A. Schubnel (2024). Change of deep subduction seismicity after a large megathrust earthquake. *Nature Communications*, **15**(1), 60. DOI: `https://doi.org/10.1038/s41467-023-43935-3`.

Geist, E. L. and P. J. Lynett (2014). Source processes for the probabilistic assessment of tsunami hazards. *Oceanography*, **27**(2), 86–93. DOI: `https://doi.org/10.5670/oceanog.2014.43`.

Goebel, T., Z. Rosson, E. Brodsky, and J. Walter (2019). Aftershock deficiency of induced earthquake sequences during rapid mitigation efforts in Oklahoma. *Earth and Planetary Science Letters*, **522**, 135–143. DOI: `https://ui.adsabs.harvard.edu/link_gateway/2019E&PSL..522..135G/doi:10.1016/j.epsl.2019.06.036`.

Gomberg, J., N. Beeler, M. Blanpied, and P. Bodin (1998). Earthquake triggering by transient and static deformations. *Journal of Geophysical Research: Solid Earth*, **103**(B10), 24411–24426. DOI: `https://doi.org/10.1029/98JB01125`.

Guo, J., Y. Li, Y. Huang, H. Deng, S. Xu, and J. Ning (2004). Green's function of the deformation of the Earth as a result of atmospheric loading. *Geophysical* *journal international*, **159**(1), 53–68. DOI: https://doi.org/10.1111/j.1365-246X.2004.02410.x.

Gutenberg, B. and C. F. Richter (1944). Frequency of earthquakes in California. *Bulletin of the Seismological society of America*, **34**(4), 185–188.

Halpaap, F., S. Rondenay, A. Perrin, S. Goes, L. Ottemöller, H. Austrheim, R. Shaw, and T. Eeken (2019). Earthquakes track subduction fluids from slab source to mantle wedge sink. *Science Advances*, **5**(4), eaav7369. DOI: https://doi.org/10.1126/sciadv.aav7369.

Hardebeck, J. L. (2012). Coseismic and postseismic stress rotations due to great subduction zone earthquakes. *Geophysical Research Letters*, **39**(21). DOI: https://doi.org/10.1029/2012GL053438.

— (2015). Stress orientations in subduction zones and the strength of subduction megathrust faults. *Science*, **349**(6253), 1213–1216. DOI: https://doi.org/10.1126/science.aac5625.

— (2017). The spatial distribution of earthquake stress rotations following large subduction zone earthquakes. *Earth, Planets and Space*, **69**(1), 69. DOI: 10.1186/s40623-017-0654-y.

Hardebeck, J. L. and A. J. Michael (2006). Damped regional-scale stress inversions: Methodology and examples for southern California and the Coalinga aftershock sequence. *Journal of Geophysical Research: Solid Earth*, **111**(B11). DOI: https://doi.org/10.1029/2005JB004144.

Hardebeck, J. L. and T. Okada (2018). Temporal stress changes caused by earthquakes: A review. *Journal of Geophysical Research: Solid Earth*, **123**(2), 1350–1365. DOI: https://doi.org/10.1002/2017JB014617.

Harris, R. A. (2017). Large earthquakes and creeping faults. *Reviews of Geophysics*, **55**(1), 169–198. DOI: https://doi.org/10.1002/2016RG000539.

Hasegawa, A., K. Yoshida, Y. Asano, T. Okada, T. Iinuma, and Y. Ito (2012). Change in stress field after the 2011 great Tohoku-Oki earthquake. *Earth and Planetary Science Letters*, **355**, 231–243. DOI: https://doi.org/10.1016/j.epsl.2012.08.042.

Hayes, G. P., G. L. Moore, D. E. Portner, M. Hearne, H. Flamme, M. Furtney, and G. M. Smoczyk (2018). Slab2, a comprehensive subduction zone geometry model. *Science*, **362**(6410), 58–61. DOI: https://doi.org/10.1126/science.aat4723.

Heidbach, O., M. Rajabi, X. Cui, K. Fuchs, B. Müller, J. Reinecker, K. Reiter, M. Tingay, F. Wenzel, F. Xie, et al. (2018). The World Stress Map database release 2016: Crustal stress pattern across scales. *Tectonophysics*, **744**, 484–498. DOI: https://doi.org/10.1016/j.tecto.2018.07.007.

Heki, K. (2003). Snow load and seasonal variation of earthquake occurrence in Japan. *Earth and Planetary Science Letters*, **207**(1-4), 159–164. DOI: 10.1016/S0012-821X(02)01148-2.

Heki, K. and S. Jin (2023). Geodetic study on earth surface loading with GNSS and GRACE. *Satellite Navigation*, **4**(1), 24. DOI: https://doi.org/10.1186/s43020-023-00113-6.

Herman, M. W. and R. Govers (2020). Stress evolution during the megathrust earthquake cycle and its role in triggering extensional deformation in subduction zones. *Earth and Planetary Science Letters*, **544**, 116379. DOI: https://doi.org/10.1016/j.epsl.2020.116379.

Hersbach, H., B. Bell, P. Berrisford, S. Hirahara, A. Horányi, J. Muñoz-Sabater, J. Nicolas, C. Peubey, R. Radu, D. Schepers, et al. (2020). The ERA5 global reanalysis. *Quarterly journal of the royal meteorological society*, **146**(730), 1999–2049. DOI: https://doi.org/10.1002/qj.3803.

Hsu, Y.-J., R. Bürgmann, Z. Jiang, C.-H. Tang, C. W. Johnson, D.-Y. Chen, H.-H. Huang, M. Tang, and X. Yang (2025). Hydrologically-induced crustal stress changes and their association with seismicity rates in Taiwan. *Earth and Planetary Science Letters*, **651**, 119181. DOI: https://doi.org/10.1016/j.epsl.2024.119181.

Hsu, Y.-J., H. Kao, R. Bürgmann, Y.-T. Lee, H.-H. Huang, Y.-F. Hsu, Y.-M. Wu, and J. Zhuang (2021). Synchronized and asynchronous modulation of seismicity by hydrological loading: A case study in Taiwan. *Science Advances*, **7**(16), eabf7282. DOI: https://doi.org/10.1126/sciadv.abf7282.

Humphrey, V., L. Gudmundsson, and S. I. Seneviratne (2016). Assessing global water storage variability from GRACE: Trends, seasonal cycle, subseasonal anomalies and extremes. *Surveys in geophysics*, **37**(2), 357–395. DOI: https://doi.org/10.1007/s10712-016-9367-1.

Ismail-Zadeh, A. T. (2013). Earthquake prediction and forecasting. *Encyclopedia of Earth Sciences Series*, 225–231. DOI: https://doi.org/10.1007/978-1-4020-4399-4_106.

Jamtveit, B., Y. Ben-Zion, F. Renard, and H. Austrheim (2018). Earthquake-induced transformation of the lower crust. *Nature*, **556**(7702), 487–491. DOI: https://doi.org/10.1038/s41586-018-0045-y.

Johnson, C. W., Y. Fu, and R. Bürgmann (2017). Seasonal water storage, stress modulation, and California seismicity. *Science*, **356**(6343), 1161–1164. DOI: https://doi.org/10.1126/science.aak9547.

Johnson, C. W., Y. Fu, and R. Bürgmann (2020). Hydrospheric modulation of stress and seismicity on shallow faults in southern Alaska. *Earth and Planetary Science Letters*, **530**, 115904. DOI: 10.1016/j.epsl.2019.115904.

Jordan, T. H., Y.-T. Chen, P. Gasparini, R. Madariaga, I. Main, W. Marzocchi, G. Papadopoulos, G. Sobolev, K. Yamaoka, and J. Zschau (2011). Operational earthquake forecasting. State of knowledge and guidelines for utilization. *Annals of Geophysics*, **54**(4). DOI: https://doi.org/10.4401/ag-5350.

Kanamori, H. and E. E. Brodsky (2004). The physics of earthquakes. *Reports on progress in physics*, **67**(8), 1429–1496. DOI: 10.1088/0034-4885/67/8/R03.

Karato, S.-i. and B. B. Karki (2001). Origin of lateral variation of seismic wave velocities and density in the deep mantle. *Journal of Geophysical Research: Solid Earth*, **106**(B10), 21771–21783. DOI: https://doi.org/10.1029/2001jb000214.

Kasahara, J. (2002). Tides, earthquakes, and volcanoes. *Science*, **297**(5580), 348–349. DOI: https://doi.org/10.1126/science.1074601.

King, G. C., R. S. Stein, and J. Lin (1994). Static stress changes and the triggering of earthquakes. *Bulletin of the Seismological Society of America*, **84**(3), 935–953. DOI: https://doi.org/10.1785/BSSA0840030935.

Kisslinger, C. (1996). Aftershocks and fault-zone properties. *Advances in geophysics*, **38**, 1–36. DOI: https://doi.org/10.1016/S0065-2687(08)60019-9.

Kita, S., H. Houston, S. Yabe, S. Tanaka, Y. Asano, T. Shibutani, and N. Suda (2021). Effects of episodic slow slip on seismicity and stress near a subduction-zone megathrust. *Nature Communications*, **12**(1), 7253. DOI: 10.1038/s41467-021-27453-8.

Klemanna, V., M. Thomasa, and H. Schuha (2014). "Elastic and Viscoelastic Response of the Lithosphere to Surface Loading". *Handbook of Geomathematics*. Ed. by W. Freeden, M. Z. Nashed, and T. Sonar. Berlin, Heidelberg: Springer Berlin Heidelberg, pp. 1–15. ISBN: 978-3-642-27793-1. DOI: 10.1007/978-3-642-27793-1_90-1. URL: https://doi.org/10.1007/978-3-642-27793-1_90-1.

Kopp, H. (2013). Invited review paper: The control of subduction zone structural complexity and geometry on margin segmentation and seismicity. *Tectonophysics*, **589**, 1–16. DOI: https://doi.org/10.1016/j.tecto.2012.12.037.

Landerer, F. W., F. M. Flechtner, H. Save, F. H. Webb, T. Bandikova, W. I. Bertiger, S. V. Bettadpur, S. H. Byun, C. Dahle, H. Dobslaw, et al. (2020). Extending the global mass change data record: GRACE follow-on instrument and science data performance. *Geophysical Research Letters*, **47**(12), e2020GL088306. DOI: https://doi.org/10.1029/2020GL088306.

Landerer, F. W. and S. S. Cooley (May 2021). *Gravity Recovery and Climate Experiment Follow-on (GRACE-FO) Level-3 Data Product User Handbook*. Tech. rep. GRACE D-103133. Jet Propulsion Laboratory, California Institute of Technology. URL: https://www.earthdata.nasa.gov/s3fs-public/2025-12/GRACE-FO_L3_Handbook_JPL.pdf?VersionId=y14PfQP3hI9QZQXl6s5Cil6jzA_auZX0.

Lapadat, Alexandru Mihai, Hubert Pierzchała, Osmari Aponte, Yiting Cai, Iwona Kudłacik, Eduard Ilie Nastase, Maciej Lackowski, and Jan Kapłon (2026). Automatic S-wave arrival timing in GNSS instantaneous velocity data. *Journal of Geodesy*. under revision.

Liu, C., A. T. Linde, and I. S. Sacks (2009). Slow earthquakes triggered by typhoons. *Nature*, **459**(7248), 833–836. DOI: https://doi.org/10.1038/nature08042.

Llenos, A. L., J. J. McGuire, and Y. Ogata (2009). Modeling seismic swarms triggered by aseismic transients. *Earth and Planetary Science Letters*, **281**(1-2), 59–69. DOI: https://doi.org/10.1016/j.epsl.2009.02.011.

Loomis, B. D., D. Felikson, T. J. Sabaka, and B. Medley (2021). High-spatial-resolution mass rates from GRACE and GRACE-FO: Global and ice sheet analyses. *Journal of Geophysical Research: Solid Earth*, **126**(12), e2021JB023024. DOI: https://doi.org/10.1029/2021JB023024.

Lowry, A. R. (2006). Resonant slow fault slip in subduction zones forced by climatic load stress. *Nature*, **442**(7104), 802–805. DOI: https://doi.org/10.1038/nature05055.

Lu, Z., H. Yi, and L. Wen (2018). Loading-induced Earth's stress change over time. *Journal of Geophysical Research: Solid Earth*, **123**(5), 4285–4306. DOI: https://doi.org/10.1029/2017JB015243.

Marsan, D. and O. Lengline (2008). Extending earthquakes' reach through cascading. *Science*, **319**(5866), 1076–1079. DOI: https://doi.org/10.1126/science.1148783.

Martens, H. R., D. F. Argus, C. Norberg, G. Blewitt, T. A. Herring, A. W. Moore, W. C. Hammond, and C. Kreemer (2020). Atmospheric pressure loading in GPS positions: Dependency on GPS processing methods and effect on assessment of seasonal deformation in the contiguous USA and Alaska. *Journal of Geodesy*, **94**(12), 115. DOI: https://doi.org/10.1007/s00190-020-01445-w.

Martens, H. R., L. Rivera, and M. Simons (2019). LoadDef: A Python-based toolkit to model elastic deformation caused by surface mass loading on spherically symmetric bodies. *Earth and Space Science*, **6**(2), 311–323. DOI: https://doi.org/10.1029/2018EA000462.

McLaskey, G. C. (2019). Earthquake initiation from laboratory observations and implications for foreshocks. *Journal of Geophysical Research: Solid Earth*, **124**(12), 12882–12904. DOI: https://doi.org/10.1029/2019JB018363.

Mignan, A. and J. Woessner (2012). Estimating the magnitude of completeness for earthquake catalogs. *Community Online Resource for Statistical Seismicity Analysis*, 1–45. DOI: https://doi.org/10.5078/corssa-00180805.

Mikolaj, M., B. Meurers, and A. Güntner (2016). Modelling of global mass effects in hydrology, atmosphere and oceans on surface gravity. *Computers & Geosciences*, **93**, 12–20. DOI: http://doi.org/10.1016/j.cageo.2016.04.014.

Moein, M. J., C. Langenbruch, R. Schultz, F. Grigoli, W. L. Ellsworth, R. Wang, A. P. Rinaldi, and S. Shapiro (2023). The physical mechanisms of induced earthquakes. *Nature Reviews Earth & Environment*, **4**(12), 847–863. DOI: https://doi.org/10.1038/s43017-023-00497-8.

Morishige, M. and S. Honda (2013). Mantle flow and deformation of subducting slab at a plate junction. *Earth and Planetary Science Letters*, **365**, 132–142. DOI: https://doi.org/10.1016/j.epsl.2013.01.033.

Mulargia, F., P. B. Stark, and R. J. Geller (2017). Why is probabilistic seismic hazard analysis (PSHA) still used? *Physics of the Earth and Planetary Interiors*, **264**, 63–75. DOI: https://doi.org/10.1016/j.pepi.2016.12.002.

Münchmeyer, J., D. Molina-Ormazabal, M. Radiguet, D. Marsan, J.-C. Baez, F. Ortega-Culaciati, A. Tassara, M. Moreno, and A. Socquet (2025). Seismic swarms unveil the mechanisms driving shallow slow slip dynamics in the copiapó ridge, northern Chile. *Geophysical Research Letters*, **52**(8), e2024GL113953. DOI: https://doi.org/10.1029/2024GL113953.

Nakata, R., N. Suda, and H. Tsuruoka (2008). Non-volcanic tremor resulting from the combined effect of Earth tides and slow slip events. *Nature Geoscience*, **1**(10), 676–678. DOI: https://doi.org/10.1038/ngeo288.

Okal, E. A. (2011). *Earthquake, Focal Mechanism.* Encyclopedia of Solid Earth Geophysics. Springer. DOI: 10.1007/978-90-481-8702-7_158.

Pagani, M., D. Monelli, G. Weatherill, L. Danciu, H. Crowley, V. Silva, P. Henshaw, L. Butler, M. Nastasi, L. Panzeri, et al. (2014). OpenQuake engine: An open hazard (and risk) software for the global earthquake model. *Seismological Research Letters*, **85**(3), 692–702. DOI: 10.1785/0220130087.

Peltier, W. R., D. Argus, and R. Drummond (2015). Space geodesy constrains ice age terminal deglaciation: The global ICE-6G_C (VM5a) model. *Journal of Geophysical Research: Solid Earth*, **120**(1), 450–487. DOI: https://doi.org/10.1002/2014JB011176.

Petricca, P. and E. Carminati (2016). Present-day stress field in subduction zones: Insights from 3D viscoelastic models and data. *Tectonophysics*, **667**, 48–62. DOI: https://doi.org/10.1016/j.tecto.2015.11.010.

Pignalberi, F., C. Giorgetti, C. Noël, C. Marone, C. Collettini, and M. M. Scuderi (2024). The effect of normal stress oscillations on fault slip behavior near the stability transition from stable to unstable motion. *Journal of Geophysical Research: Solid Earth*, **129**(2), e2023JB027470. DOI: https://doi.org/10.1029/2023jb027470.

Prodehl, C., B. Kennett, I. M. Artemieva, and H. Thybo (2013). 100 years of seismic research on the Moho. *Tectonophysics*, **609**, 9–44. DOI: https://doi.org/10.1016/j.tecto.2013.05.036.

Reasenberg, P. (1985). Second-order moment of central California seismicity, 1969–1982. *Journal of Geophysical Research: Solid Earth*, **90**(B7), 5479–5495. DOI: https://doi.org/10.1029/JB090iB07p05479.

Rodell, M., P. Houser, U. Jambor, J. Gottschalck, K. Mitchell, C.-J. Meng, K. Arsenault, B. Cosgrove, J. Radakovich, M. Bosilovich, et al. (2004). The global land data assimilation system. *Bulletin of the American Meteorological society*, **85**(3), 381–394. DOI: https://doi.org/10.1175/BAMS-85-3-381.

Romanowicz, B. (2003). Global mantle tomography: progress status in the past 10 years. *Annual Review of Earth and Planetary Sciences*, **31**(1), 303–328. DOI: https://doi.org/10.1146/annurev.earth.31.091602.113555.

Rontogianni, S., K. Konstantinou, N. Melis, and C. Evangelidis (2011). Slab stress field in the Hellenic subduction zone as inferred from intermediate-depth earthquakes. *Earth, planets and space*, **63**(2), 139–144. DOI: https://doi.org/10.5047/eps.2010.11.011.

Royer, A., A. Roy, S. Jutras, and A. Langlois (2021). Performance assessment of radiation-based field sensors for monitoring the water equivalent of snow cover (SWE). *The Cryosphere*, **15**(11), 5079–5098. DOI: https://doi.org/10.5194/tc-15-5079-2021.

Salstein, D. A., R. M. Ponte, and K. Cady-Pereira (2008). Uncertainties in atmospheric surface pressure fields from global analyses. *Journal of Geophysical Research: Atmospheres*, **113**(D14). DOI: https://doi.org/10.1029/2007JD009531.

Save, H., S. Bettadpur, and B. D. Tapley (2016). High-resolution CSR GRACE RL05 mascons. *Journal of Geophysical Research: Solid Earth*, **121**(10), 7547–7569. DOI: https://doi.org/10.1002/2016JB013007.

Scholz, C. H. (2019). *The mechanics of earthquakes and faulting*. Cambridge university press. ISBN: 9780521652230]. DOI: 10.1017/CBO9780511818516.

Scire, A., G. Zandt, S. Beck, M. Long, and L. Wagner (2017). The deforming Nazca slab in the mantle transition zone and lower mantle: Constraints from teleseismic tomography on the deeply subducted slab between 6 S and 32 S. *Geosphere*, **13**(3), 665–680. DOI: https://doi.org/10.1130/GES01436.1.

Shaw, B. and J. Jackson (2010). Earthquake mechanisms and active tectonics of the Hellenic subduction zone. *Geophysical Journal International*, **181**(2), 966–984. DOI: 10.1111/j.1365-246X.2010.04551.x.

Shearer, P. M. (2019). *Introduction to Seismology*. Cambridge university press. ISBN: 978-1-107-18447-3.

Sippl, C., A. Dielforder, T. John, and S. M. Schmalholz (2022). Global constraints on intermediate-depth intraslab stresses from slab geometries and mechanisms of double seismic zone earthquakes. *Geochemistry, Geophysics, Geosystems*, **23**(9), e2022GC010498. DOI: https://doi.org/10.1029/2022GC010498.

Sippl, C., B. Schurr, J. Münchmeyer, S. Barrientos, and O. Oncken (2023). The Northern Chile forearc constrained by 15 years of permanent seismic monitoring. *Journal of South American Earth Sciences*, **126**, 104326. DOI: https://doi.org/10.1016/j.jsames.2023.104326.

Smith-Konter, B. and D. Sandwell (2009). Stress evolution of the San Andreas fault system: Recurrence interval versus locking depth. *Geophysical Research Letters*, **36**(13). DOI: https://doi.org/10.1029/2009GL037235.

Steffen, R. and H. Steffen (2021). Reactivation of non-optimally orientated faults due to glacially induced stresses. *Tectonics*, **40**(11), e2021TC006853. DOI: 10.1029/2021TC006853.

Stein, R. S. (1999). The role of stress transfer in earthquake occurrence. *Nature*, **402**(6762), 605–609. DOI: 10.1038/45144.

Stern, R. J. (2002). Subduction zones. *Reviews of geophysics*, **40**(4), 3–1. DOI: https://doi.org/10.1029/2001RG000108.

Stiphout, T. van, J. Zhuang, and D. Marsan (2012). Seismicity declustering. *Community online resource for statistical seismicity analysis*, **10**(1), 1–25. DOI: http://dx.doi.org/10.5078/corssa-52382934.

Tapley, B. D., S. Bettadpur, M. Watkins, and C. Reigber (2004). The gravity recovery and climate experiment: Mission overview and early results. *Geophysical research letters*, **31**(9). DOI: https://doi.org/10.1029/2004GL019920.

Thomas, M. (2002). "Ocean induced variations of Earths rotation–Results from a simultaneous model of global circulation and tides". PhD thesis. Ph. D. diss., 129 pp., Univ. of Hamburg, Germany.

Toda, S., R. S. Stein, G. C. Beroza, and D. Marsan (2012). Aftershocks halted by static stress shadows. *Nature Geoscience*, **5**(6), 410–413. DOI: https://doi.org/10.1038/NGEO1465.

Turcotte, D. L. and G. Schubert (2002). *Geodynamics*. Cambridge university press. ISBN: 0-521-66186-2.

Uhrhammer, R. (1986). Characteristics of northern and central California seismicity. *Earthquake Notes*, **57**(1), 21.

UNDRR (2026). *Earthquake day*. [Online; accessed 17-Apr-2026]. URL: https://www.undrr.org/m/earthquake-day/.

Vidale, J. E., D. C. Agnew, M. J. Johnston, and D. H. Oppenheimer (1998). Absence of earthquake correlation with Earth tides: An indication of high preseismic fault stress rate. *Journal of Geophysical Research: Solid Earth*, **103**(B10), 24567–24572. DOI: https://doi.org/10.1029/98JB00594.

Wang, L. and S. Barbot (2023). Three-dimensional kinematics of the India–Eurasia collision. *Communications Earth & Environment*, **4**(1), 164. DOI: https://doi.org/10.1038/s43247-023-00815-4.

Watkins, M. M., D. N. Wiese, D.-N. Yuan, C. Boening, and F. W. Landerer (2015). Improved methods for observing Earth's time variable mass distribution with GRACE using spherical cap mascons. *Journal of Geophysical Research: Solid Earth*, **120**(4), 2648–2671. DOI: https://doi.org/10.1002/2014JB011547.

WHO (2026). *WHO*. [Online; accessed 17-Apr-2026]. URL: https://www.who.int/health-topics/earthquakes#tab=tab_1.

Wiemer, S. (2001). A software package to analyze seismicity: ZMAP. *Seismological Research Letters*, **72**(3), 373–382. DOI: https://doi.org/10.1785/gssrl.72.3.373.

Wiemer, S. and M. Wyss (2000). Minimum magnitude of completeness in earthquake catalogs: Examples from Alaska, the western United States, and Japan. *Bulletin of the Seismological Society of America*, **90**(4), 859–869. DOI: https://doi.org/10.1785/0119990114.

Xue, L., Y. Fu, and H. R. Martens (2021). Seasonal hydrological loading in the Great Lakes region detected by GNSS: A comparison with hydrological models. *Geophysical Journal International*, **226**(2), 1174–1186. DOI: https://doi.org/10.1093/gji/ggab158.

Yoshida, K., A. Hasegawa, T. Okada, T. Iinuma, Y. Ito, and Y. Asano (2012). Stress before and after the 2011 great Tohoku-oki earthquake and induced earthquakes in inland areas of eastern Japan. *Geophysical Research Letters*, **39**(3). DOI: https://doi.org/10.1029/2011GL049729.

Zaliapin, I. and Y. Ben-Zion (2013). Earthquake clusters in southern California I: Identification and stability. *Journal of Geophysical Research: Solid Earth*, **118**(6), 2847–2864. DOI: 10.1002/jgrb.50179.

— (2020). Earthquake declustering using the nearest-neighbor approach in space-time-magnitude domain. *Journal of Geophysical Research: Solid Earth*, **125**(4), e2018JB017120. DOI: https://doi.org/10.1029/2018JB017120.

Zhao, W., F. Amelung, M.-P. Doin, T. H. Dixon, S. Wdowinski, and G. Lin (2016). InSAR observations of lake loading at Yangzhuoyong Lake, Tibet: Constraints on crustal elasticity. *Earth and Planetary Science Letters*, **449**, 240–245. DOI: https://doi.org/10.1016/j.epsl.2016.05.044.

Zheng, G., H. Wang, T. J. Wright, Y. Lou, R. Zhang, W. Zhang, C. Shi, J. Huang, and N. Wei (2017). Crustal deformation in the India-Eurasia collision zone from 25 years of GPS measurements. *Journal of Geophysical Research: Solid Earth*, **122**(11), 9290–9312. DOI: https://doi.org/10.1002/2017JB014465.

Zhuang, J., Y. Ogata, and D. Vere-Jones (2002). Stochastic declustering of space-time earthquake occurrences. *Journal of the American Statistical Association*, **97**(458), 369–380. DOI: https://doi.org/10.1198/016214502760046925.

Zoback, M. L. (1992). First-and second-order patterns of stress in the lithosphere: The World Stress Map Project. *Journal of Geophysical Research: Solid Earth*, **97**(B8), 11703–11728. DOI: https://doi.org/10.1029/92JB00132.